

# 1 Defective *Slc7a7* transport reduces systemic arginine 2 availability compromising erythropoiesis and iron 3 homeostasis

4  
5  
6 Fernando Sotillo<sup>1\*</sup>, Judith Giroud-Gerbetant<sup>1,2\*</sup>, Jorge Couso<sup>3</sup>, Rafael Artuch<sup>2,4,5</sup>,  
7 Antonio Zorzano<sup>1,6,7</sup>, Aida Ormazabal<sup>2,6,7</sup>, Mayka Sanchez<sup>8</sup>, Günter Weiss<sup>9</sup>, Susanna  
8 Bodoy<sup>1,2,10#</sup>, Manuel Palacín<sup>1,2,4#</sup>

9  
10 <sup>1</sup>Institute for Research in Biomedicine Barcelona (IRB Barcelona), Barcelona, Spain;  
11 <sup>2</sup>Centro de Investigación Biomédica en Red Enfermedades Raras (CIBERER),  
12 Barcelona, Spain; <sup>3</sup>Institute of Predictive and Personalized Medicine of Cancer,  
13 Badalona, Spain; <sup>4</sup>Department of Clinical Biochemistry, Hospital Sant Joan de Déu  
14 (HSJD), Esplugues de Llobregat, Spain; <sup>5</sup>Institut de Recerca Sant Joan de Déu,  
15 Esplugues de Llobregat, Spain; <sup>6</sup>Department of Biochemistry and Molecular  
16 Biomedicine, University of Barcelona, Barcelona, Spain; <sup>7</sup>Centro de Investigación  
17 Biomédica en Red Diabetes y Enfermedades Metabólicas (CIBERDEM), Spain;  
18 <sup>8</sup>Faculty of Medicine and Health Sciences. Universitat Internacional de Catalunya  
19 (UIC), Sant Cugat, Spain; <sup>9</sup>Department of Internal Medicine II (Infectious Diseases,  
20 Immunology, Rheumatology and Pneumology), Medical University of Innsbruck,  
21 Innsbruck, Austria; <sup>10</sup>Department of Biosciences, University of Vic - Central University  
22 of Catalonia, Vic, Spain.

23 \*These authors contributed equally

24 Key words: y<sup>+</sup>LAT1, arginine, iron metabolism, macrophage, red blood cell (RBC)

25 # Correspondence: [mpalacin@irbbarcelona.org](mailto:mpalacin@irbbarcelona.org) (M.P.),  
26 [susanna.bodoy@irbbarcelona.org](mailto:susanna.bodoy@irbbarcelona.org) (S.B.)

27 **ABSTRACT**

28 *Slc7a7* encodes for  $\gamma^+$ LAT1, a transporter of cationic amino acid across the basolateral  
29 membrane of epithelial cells. Mutations in *SLC7A7* gene give rise to Lysinuric Protein  
30 Intolerance (LPI), a rare autosomal recessive disease with wide variability of  
31 complications. Intriguingly,  $\gamma^+$ LAT1 is also involved in arginine transport in non-  
32 polarized cells such as macrophages. Here we report that complete inducible *Slc7a7*  
33 ablation in mouse compromises systemic arginine availability that alters proper  
34 erythropoiesis and that dysfunctional RBC generation leads to increased  
35 erythrophagocytosis, iron overload and an altered iron metabolism by macrophages.  
36 Herein, uncovering a novel mechanism that links amino acid metabolism to  
37 erythropoiesis and iron metabolism. Mechanistically, the iron exporter ferroportin-1  
38 expression was compromised by increased plasma hepcidin causing macrophage iron  
39 accumulation. Strikingly, lysozyme M-cell-specific knockout mice failed to reproduce  
40 the total knockout alterations, while bone marrow transplantation experiments resulted  
41 in the resolution of macrophage iron overload but could not overcome erythropoietic  
42 defect. This study establishes a new crucial link between systemic arginine availability  
43 in erythropoiesis and iron homeostasis.

44  
45  
46  
47  
48  
49  
50  
51  
52  
53  
54  
55  
56  
57

58 **Introduction**

59 Red blood cell (RBC) generation is a tightly regulated process where RBC  
60 homeostasis is key for proper iron recycling (de Back et al., 2014). Although extensive  
61 work has been done in the field of erythropoiesis, little is known about the impact of  
62 amino acid metabolism in this complex process. The mechanisms of RBC generation  
63 spans from bone marrow (BM) erythroid differentiation mediated by CD169<sup>+</sup>  
64 macrophages (Chow et al., 2013), which supports erythroblastic island formation, to  
65 the end-final stage where RBC phagocytosis by red pulp macrophages (RPMs) leads  
66 to hemoglobin breakdown and ultimately iron recycling and release (Klei et al., 2017).  
67 RBC maturation requires specific components to properly coordinate this process.  
68 Disruption in hemoglobin synthesis, which comprises one-third of the RBC protein  
69 content, leads to altered erythropoiesis (Kuhn et al., 2017; Liu et al., 2013) . Yet,  
70 hemoglobin is not the only key component as iron, erythropoietin (EPO), or ferritin are  
71 also well known to play essential roles in RBC generation (Beguin, 1998; Goldfarb et  
72 al., 2021; Moritz et al., 1997). In terms of metabolic requirements, Shima et al.  
73 published the impact of arginine import on erythrocyte differentiation and proliferation  
74 throughout the cationic amino acid transporter 1 (CAT1), thereby indicating a crucial  
75 role not only of the iron-related components (hemoglobin, EPO, iron and ferritin) but  
76 also of metabolites such as arginine in the generation of mature RBCs (Shima et al.,  
77 2006). Macrophages also play an important role in RBC enucleation, being thus key  
78 for the last step of RBC generation (Lee et al., 2004; Popova et al., 2009; Swartz et  
79 al., 2017).  
80 Macrophages are a cell type that participates in diverse biological processes, including  
81 host defence and wound repair (Koh and DiPietro, 2011). Nevertheless, further roles  
82 for these cells began to emerge with the identification of specific functions of tissue-

83 resident macrophages, such as Kupffer cells and splenic RPMs, which are mainly  
84 involved in erythrocyte phagocytosis and iron recycling (Beaumont and Delaby, 2009;  
85 Ganz, 2012; Theurl et al., 2016), alveolar macrophages (AMs), which participate in  
86 both lung development and surfactant recycling, and osteoclasts, which contribute to  
87 bone development (Hussell and Bell, 2014; Murray and Wynn, 2011). Interest in  
88 macrophages in the context of metabolic disease has gained momentum due to a  
89 number of recent findings. Macrophage polarization is well known to be tightly linked  
90 to altered cellular metabolism including iron homeostasis and glycolysis/citric acid  
91 cycle activity (Recalcati et al., 2012; Stienstra et al., 2017). In addition, changes in L-  
92 arginine metabolism have been coupled to different immune effector phenotypes of  
93 macrophages involved in autoimmunity, infection control and activation (Bronte and  
94 Zanovello, 2005; Jha et al., 2015; Weiss and Schaible, 2015).

95 Lysinuric Protein Intolerance (LPI, MIM 222700) is a rare autosomal recessive disease  
96 caused by mutations in *SLC7A7* gene (solute carrier family 7) which encodes for  
97  $\gamma^+$ LAT1 (Palacín et al., 2001; Torrents et al., 1999), a light subunit of the heterodimeric  
98 amino acid transporter family.  $\gamma^+$ LAT1 mediates the exchange of cationic amino acids  
99 (CAAs) with neutral amino acids plus sodium (Palacín et al., 2005) across the  
100 basolateral membrane of epithelial cells. Mutations in  $\gamma^+$ LAT1 results in defective  
101 transport of CAAs, leading to reduced arginine, ornithine and lysine plasma  
102 concentration while increased in urine (Ogier de Baulny et al., 2012). Consistent with  
103 the clinical manifestations of human LPI, we have previously reported that the  
104 inducible complete loss of  $\gamma^+$ LAT1 in mice leads to hypoargininemia, which results in  
105 urea cycle disruption and hyperammonemia. Consequently leading to reduced body  
106 weight, brain edema and pulmonary alveolar proteinosis between other complications  
107 (Bodoy et al., 2019). In addition, several studies found that patients with one or several

108 mutations in *S/c7a7* gene have abnormal blood count, as well as microcytic anemia  
109 (Alqarajeh et al., 2020; Rajantie et al., 1980). To date, the standard treatment for LPI  
110 mainly consists on a low-protein based diet supplemented with oral citrulline  
111 (Lukkarinen et al., 2003), where citrulline is intracellularly converted to arginine in renal  
112 epithelial cells. Hence, improving the defects in urea cycle and correcting both plasma  
113 arginine and ammonia levels (Dhanakoti et al., 1990).  
114 Notably,  $\gamma^+$ LAT1 also mediates arginine transport in non-polarized cells, such as  
115 macrophages. Intriguingly,  $\gamma^+$ LAT1 was shown to drive major arginine transport in  
116 human monocytes after interferon stimulation (Rotoli et al., 2020). Thus, being one of  
117 the major arginine transporters in human monocytes, AMs and monocyte-derived  
118 macrophages (Barilli et al., 2012).  
119 Motivated by the fact that human SLC7A7 mutations give rise to immune and  
120 hematological complications, here we questioned whether amino acid transport via  
121 *S/c7a7* has important roles for erythropoiesis and/or iron homeostasis. Using total  
122 loss-of-function of  $\gamma^+$ LAT1, recovery with citrulline, Lysozyme M-cell-specific (i.e.  
123 myeloid-specific) knockout mice and BM transplantations, we demonstrated that the  
124 systemic metabolic condition of LPI (mainly hypoargininemia and/or  
125 hyperammonemia) leads to defective erythropoiesis and altered RBCs, prompting  
126 thus increased erythrophagocytosis ultimately leading to highly iron loaded RPMs and  
127 BMMs and hyperferritinemia. Mechanistically, depletion of extracellular arginine and  
128 increased plasma ammonia levels, as a result of *S/c7a7* ablation in kidney and intestine,  
129 leads to impaired development of RBCs that are more phagocytized by RPMs. Iron  
130 overload is a well known hepcidin driver through the bone morphogenic protein – 6  
131 (BMP6) (Andriopoulos et al., 2009), hence, high levels of iron triggered hepcidin  
132 expression which in turn downregulated FPN1 in *S/c7a7* macrophages, by this way

133 altering iron recycling. Further analyses revealed that defective erythropoiesis was  
134 absent in the myeloid-specific knockout mouse. These findings connect two previously  
135 unrelated biological processes, namely defective RBC generation and macrophage  
136 iron accumulation, and implicate the LPI metabolic derangement as a key player in the  
137 hematologic complications of the disease.

138 **Results**

139 **Global y<sup>+</sup>LAT1 ablation in adult mice results in a drastic reduction of bone**  
140 **marrow macrophages and red pulp macrophages.**

141 Y<sup>+</sup>LAT1 is highly expressed in epithelial cells and in some non-polarized cells such as  
142 macrophages (Pollard, 2009; Rotoli et al., 2020). To dissect the role of y<sup>+</sup>LAT1 in the  
143 immune and hematological complications of LPI, we created a y<sup>+</sup>LAT1 conditional  
144 allele (*Slc7a7*<sup>loxp/+</sup>) and generated a *Slc7a7*<sup>loxp/loxp/UBC-Cre<sup>+</sup> inducible knockout model  
145 that expresses Cre in all the body cells in response to tamoxifen treatment. Twelve-  
146 week-old *Slc7a7*<sup>loxp/loxp/UBC-Cre<sup>+</sup> (*Slc7a7*<sup>-/-</sup>, after tamoxifen induction) mice and their  
147 control *Slc7a7*<sup>loxp/loxp/UBC-Cre<sup>-</sup> (*Slc7a7*<sup>+/+</sup>) littermates were first treated with tamoxifen for  
148 7 days to induce Cre expression and were further kept on low-protein diet. As a result,  
149 y<sup>+</sup>LAT1 depletion led to significant reduction of spleen weight (Figure 1A). However,  
150 consistent with previous reports that citrulline administration ameliorates  
151 hypoargininemia and hyperammonemia as well as the vast majority of the defects  
152 caused by y<sup>+</sup>LAT1 ablation (Bodoy et al., 2019), 10 days of citrulline supplementation  
153 also improved spleen weight (Supplementary Figure 1A). Of note, *Slc7a7* ablation led  
154 to lower levels of F4/80-positive cells in spleen and BM sections, together with a  
155 reduced number of F4/80<sup>hi</sup> cd11b<sup>lo</sup> cells *in vivo* (Figure 1B-C), which were also  
156 recovered by citrulline administration (Supplementary Figure 1B-C). Besides,</sup></sup></sup>

157 circulating monocytes levels were also decreased in  $\gamma^+$ LAT1-deficient mice, thereby  
158 indicating a loss of macrophage precursors (Figure 1D).

159 We then asked whether the decreased number of RPMs was associated with a  
160 reduced proliferation or increased apoptosis. To this end, we assessed Ki67 and  
161 caspase-3 expression in spleen sections. Indeed, Ki67 was reduced in the red pulp  
162 area of  $Slc7a7^{-/-}$  mice, where RPMs reside (Figure 1E). Moreover,  $Slc7a7^{-/-}$  RPMs  
163 expressed higher levels of active caspase-3 compared with those of control mice  
164 (Figure 1F). Taken together, our data suggests that  $\gamma^+$ LAT1 participates in the  
165 homeostasis of BMMs and RPMs, which might be caused by both increased apoptosis  
166 and decreased levels of proliferation.

167

168  **$\gamma^+$ LAT1 deficiency in myeloid cell line does not reproduce conditional knockout  
169 mice deficiencies.**

170 We then asked whether the lack of  $Slc7a7$  expression in macrophages was key for the  
171 defects previously observed (Figure 1 A,C). For that purpose, we generated a myeloid  
172 cell-specific knockout mouse ( $Slc7a7^{llox/llox}$   $LysM-Cre^+$ ;  $Slc7a7^{LysM^{-/-}}$ ) in which Cre  
173 expression is specifically restricted to the myeloid cell lineage. Likewise, the inducible  
174 knockout mice,  $Slc7a7^{LysM}$ , showed a reduced expression of  $Slc7a7$  in RPMs, AMs  
175 and BMDMs (Supp Figure 2A-B). Nevertheless, contrary to the inducible model  
176  $Slc7a7^{-/-}$  (Bodoy et al., 2019),  $Slc7a7^{LysM}$  mice did not present reduction of  $\gamma^+$ LAT1  
177 expression in kidney, hypoargininemia or urea cycle dysfunction (e.g., increased orotic  
178 acid in urine), nor did they show a reduction in spleen size or body weight or a  
179 decrease in RPMs and BMMs numbers *in vivo* (Supp Figure 2B-G). These findings  
180 rule out the possibility that the defect comes from the lack of  $\gamma^+$ LAT1 expression in the  
181 myeloid cell line and embraces the possibility that systemic reduction of arginine along

182 with other unbalanced amino acids and metabolites (LPI systemic metabolic condition)  
183 might underlie the observed decrease in macrophage generation and survival in total  
184 knockout mice.

185

186 ***Slc7a7*<sup>-/-</sup> but not *Slc7a7*<sup>LysM</sup> red pulp macrophages, have a dysfunctional iron**  
187 **metabolism.**

188 Since one of the main functions of RPMs is to regulate erythrocyte degradation and  
189 iron delivery for erythropoiesis (Kohyama et al., 2009), we next focused on whether  
190 iron metabolism was compromised in both mouse models. *Slc7a7*<sup>-/-</sup> mice showed a  
191 dramatic iron accumulation in the BM and spleen. In contrast, abnormal iron  
192 accumulation was not visible in *Slc7a7*<sup>LysM</sup> animals (Figure 2A), thus, further  
193 confirming the premise that y<sup>+</sup>LAT1 deficiency in the myeloid cell line does not cause  
194 macrophage dysfunction. Citrulline treatment improved iron accumulation in the  
195 spleen and BM in *Slc7a7*<sup>-/-</sup> mouse (Figure 2A). In line with this finding, iron content in  
196 the liver and spleen tissue were higher in the *Slc7a7*<sup>-/-</sup> mice compared to its control  
197 littermates and were rescued by citrulline supplementation (Figure 2B).

198 We next addressed whether iron accumulation in tissues would also be reflected into  
199 higher serum ferritin levels (Cohen et al., 2010), a trait usually reported in LPI patients  
200 (Ogier de Baulny et al., 2012). Hyperferritinemia was found in the *Slc7a7* knockout  
201 mice (Figure 2C), and, as expected, the impairment was reversed by citrulline  
202 administration and no differences were observed in the *Slc7a7*<sup>LysM</sup> mouse model  
203 (Figure 2C). To study whether hyperferritinemia was associated with increased  
204 inflammation (Kawasumi et al., 2014; Rosário et al., 2013), we examined IL6 plasma  
205 levels. Strikingly, control and *Slc7a7*<sup>-/-</sup> mice showed similar levels of IL6 (Supp Figure  
206 3A), excluding thereby systemic inflammation as a plausible cause of increased

207 ferritinemia or macrophage iron retention (Theurl et al., 2016). Given that  $\gamma$  LAT1  
208 deletion resulted in a significant reduction in the number of RPMs and BMMs, we  
209 tested whether the observed iron accumulation was directly linked to macrophages.  
210 Of note, within the spleen, iron accumulation was specifically located in the resident  
211 RPMs (Figure 2D).

212 As a whole, these results indicate that the systemic metabolic conditions of LPI cause  
213 detrimental effects on RPM homeostasis but *Slc7a7* expression in macrophages is not  
214 required for the iron accumulation in tissue.

215

### 216 ***Slc7a7*<sup>-/-</sup> mouse model show reduced expression of FPN1 in macrophages**

217 To gain insight into how iron is accumulated in macrophages, we analyzed the  
218 expression of FPN1, the only known iron exporter, and its relationship to circulating  
219 concentrations of hepcidin, the major iron-regulatory hormone that interacts directly  
220 with FPN1 triggering its degradation (Nemeth et al., 2004). Of note, hepcidin plasma  
221 levels were increased in *Slc7a7*<sup>-/-</sup> mice (Figure 3A) which were paralleled by increased  
222 expression levels of liver hepcidin (*Hamp1*) in *Slc7a7*<sup>-/-</sup> mice as compared to control  
223 littermates (Figure 3B). Hepcidin levels can be regulated at the transcriptional levels  
224 by several factors such as inflammation and hepatocyte iron deposits (Sebastiani et  
225 al., 2016). In this regard, microarray data on sorted RPMs from *Slc7a7*<sup>+/+</sup> and *Slc7a7*  
226 <sup>-/-</sup> mouse showed decreased expression of inflammatory-related pathways. Moreover,  
227 as indicated above, plasma interleukin 6 levels showed similar levels between both  
228 genotypes, thus ruling out the possibility of inflammation as a plausible cause for  
229 increased hepcidin levels (Supplementary Figure 3A-B). Nevertheless, enhanced  
230 Pearl's Prussian blue staining revealed that *Slc7a7*<sup>-/-</sup> liver sections showed specific  
231 localization of iron deposits in hepatocytes (Figure 3C), suggesting thus iron

232 accumulation as the main cause for increased hepcidin levels. The increased number  
233 of iron deposits was accompanied by a significant increase of the BMP6 (Figure 3D),  
234 a protein known to interact with hemojuvelin to further (Core et al., 2014), trigger  
235 *Hamp1* transcription and expression (Andriopoulos et al., 2009; JL et al., 2006). Thus,  
236 further supporting the premise that hepatocyte liver accumulation triggers increased  
237 hepcidin plasma levels.

238 Flow cytometry analysis revealed a decreased number of FPN1-positive RPMs in  
239 *Slc7a7*<sup>-/-</sup> compared to wildtype mice (Figure 3E). Moreover, decreased FPN1  
240 expression in RPMs was also confirmed by western blot, where *Slc7a7*<sup>-/-</sup> mice show  
241 reduced levels of FPN1 in total spleen (Figure 3F).

242 Together, our results indicate that *Slc7a7* expression is necessary to maintain proper  
243 FPN1 expression and that its imbalance leads to an aberrant iron retention in resident  
244 macrophages.

245

#### 246 ***Slc7a7*<sup>-/-</sup> mice show exacerbated erythrophagocytosis**

247 Our findings that *Slc7a7*<sup>-/-</sup> RPM were loaded with iron together with the imbalance on  
248 iron metabolism suggests that RPM function is impaired in *Slc7a7*<sup>-/-</sup> knockout mouse.  
249 In that sense, gene expression analysis of sorted RPMs from *Slc7a7*<sup>+/+</sup> and *Slc7a7*<sup>-/-</sup>  
250 animals revealed altered expression of key RPM-associated genes (Figure 4A)  
251 (Haldar et al., 2014; Kohyama et al., 2009) further supporting an impaired RPM  
252 functioning and disrupted iron handling. Moreover, RPMs are a highly specialized  
253 erythrophagocytic cell type in which several genes have been proposed as master  
254 regulators of iron homeostasis and RBC clearance (Kohyama et al., 2009). In this  
255 regard, these animals showed increased expression of *SpiC*, the master regulator of  
256 RPM differentiation, *Msr1*, the macrophage scavenger receptor 1, and the hemoglobin

257 scavenger receptor *CD163* in *Slc7a7<sup>-/-</sup>* mice, while *Il1b* gene expression, a  
258 proinflammatory cytokine linked to erythrophagocytosis (A-Gonzalez et al., 2017; Guo  
259 et al., 2019; Kohyama et al., 2009; Oexle et al., 2003), was significantly reduced  
260 (Figure 4B) (Moestrup and Møller, 2004). This expression pattern suggested an  
261 increased erythrophagocytosis activity in *Slc7a7<sup>-/-</sup>* mice. To examine this effect in  
262 further detail, we measured the erythrophagocytosis ratio of BMDMs from wildtype and  
263 knockout mouse. Strikingly, when *Slc7a7<sup>-/-</sup>* and control RBCs were co-incubated with  
264 BMDMs from *Slc7a7<sup>-/-</sup>* or control mice, *Slc7a7<sup>-/-</sup>* erythrocytes were preferentially  
265 engulfed by both macrophages (Figure 4C). Hence, *ex vivo* experiments confirmed a  
266 significantly higher phagocytosis rate of RBCs derived from *Slc7a7<sup>-/-</sup>* deficient mice  
267 compared to RBCs from control animals. In addition, RBCs from *Slc7a7<sup>-/-</sup>* and control  
268 animals treated with citrulline were equally engulfed by both macrophages,  
269 demonstrating again the rescuing effect of citrulline (data not shown). These results  
270 indicate that the observed iron accumulation in macrophages is due to a defect on the  
271 RBCs rather than an alteration on the RPMs functioning.

272

### 273 **y<sup>+</sup>LAT1 depletion results in defective erythropoiesis**

274 To understand the mechanisms underlying the defect in erythrocytes that results in  
275 increased erythrophagocytosis (Figure 4B), we performed a hematological analysis of  
276 *Slc7a7<sup>-/-</sup>* animals and its control littermates. *Slc7a7<sup>-/-</sup>* erythrocytes had a reduced mean  
277 corpuscular volume (MCV) and hemoglobin (MCH) as well as a decreased mean  
278 platelet volume (MPV), while no differences were found in *Slc7a7<sup>LysM</sup>* mice (Figure 5A-  
279 F). Interestingly, erythropoietic progenitors analyzed by flow cytometry showed that  
280 *Slc7a7<sup>-/-</sup>* mice have a severe reduction in erythrocyte precursors (Figure 5G). The  
281 dramatic decrease in erythroid precursors implies that LPI systemic metabolic

282 condition caused by global *Slc7a7* ablation compromises RBC generation. In fact,  
283 erythroid precursors of *Slc7a7*<sup>LysM</sup> mice were not affected (Figure 5G).  
284 EPO is a secreted hormone responsible for stimulating RBC production and survival.  
285 Specifically, EPO has been described to stimulate RBC generation at the  
286 proerythroblast stage (Hattangadi et al., 2011). We therefore measured EPO plasma  
287 levels and found that, indeed, EPO levels were significantly decreased in *Slc7a7*<sup>-/-</sup>  
288 mice (Figure 5H). As a whole, these results indicate that  $\gamma^+$ LAT1 plays a specific role  
289 in erythroid development at multiple proerythroblast stages, possibly orchestrated by  
290 the metabolic defects caused by *Slc7a7* ablation.

291

292 **Bone marrow transplant improves iron accumulation but not the metabolic  
293 complications and erythropoietic defects**

294 Since immature erythroid precursors were dramatically reduced in *Slc7a7*<sup>-/-</sup> mice  
295 (Figure 5G), RBCs had an altered MCV and MCH (Figure 5D-E), and *Slc7a7*<sup>LysM</sup>  
296 animals did not show any erythropoietic defects (Figure 5A-G), we speculated that the  
297 observed alterations in the *Slc7a7*<sup>-/-</sup> background could be due to the modified systemic  
298 microenvironment rather than a cell-autonomous defect in the BM. For this purpose,  
299 BM cells isolated from *Slc7a7*<sup>+/+</sup> mice (CD45.1) were harvested and transplanted into  
300 lethally irradiated *Slc7a7*<sup>-/-</sup> mice (CD45.2); conversely, BM cells isolated from *Slc7a7*<sup>-/-</sup>  
301 mice (CD45.2) were harvested and transplanted into lethally irradiated *Slc7a7*<sup>+/+</sup>  
302 mice (CD45.1). Five weeks after transplantation, mice were placed on a tamoxifen diet  
303 for 7 days and then further fed a low-protein diet for 10 days prior to the sacrifice day  
304 (Figure 6A). In this setting, BM transplantation did not improve the body and spleen  
305 weight of the *Slc7a7*<sup>-/-</sup> animals (CD45.2) transplanted with *Slc7a7*<sup>+/+</sup> BM (CD45.1)  
306 (Figure 6B-C). Analysis of peripheral blood revealed that arginine plasma levels were

307 diminished and orotic acid levels in urine were high as a consequence of the urea  
308 cycle dysfunction (Figure 6D-E). Thus, as expected, BM transplant did not affect the  
309 main metabolic complications of LPI. Interestingly, *Slc7a7*<sup>-/-</sup> mice receiving *Slc7a7*<sup>+/+</sup>  
310 BM, did not present iron accumulation in the spleen nor differences in the MCH (Figure  
311 6F, J) and exhibited a tendency towards lower plasma ferritin levels (Figure 6G). This  
312 finding thus indicates that BM transplant can specifically rescue iron metabolism  
313 defects. Conversely, *Slc7a7*<sup>-/-</sup> transplanted mice exhibited a vast decrease in erythroid  
314 progenitors I-IV compartments together with reduced MCV (Figure 6H), reaffirming the  
315 profound systemic effect of y<sup>+</sup>LAT1 deficiency on RBC generation and homeostasis.

316

317

318 **Discussion**

319 The y<sup>+</sup>LAT1 transporter is a cationic/neutral amino acid exchanger that provides  
320 arginine for different processes in the organism. Proper arginine availability is essential  
321 for a normal urea cycle (Morris, 2002). The deficiency of y<sup>+</sup>LAT1 transporter in LPI  
322 condition, causes systemic hypoargininemia, which due to the shortage of urea cycle  
323 intermediates, results in hyperammonemia (Bodoy et al., 2019). In our mouse model  
324 of LPI, as shown here, this metabolic derangement causes erythropoiesis failure,  
325 whereas y<sup>+</sup>LAT1 expression in macrophages is not enough to cause impaired  
326 development of RBCs in the *Slc7a7*<sup>LysM</sup> mouse model. In this regard, little is known  
327 about the role of amino acid availability in erythropoiesis. The impact of L-arginine in  
328 erythrocytes is highlighted by the fact that ablation of the arginine transporter CAT1 in  
329 mouse results in perinatal death and anemia (Perkins et al., 1997) and that L-arginine-  
330 mediated CAT1 transport participates in erythrocyte differentiation and proliferation *in*  
331 *vitro* (Shima et al., 2006). Moreover, the L-arginine catalytic enzyme endothelial nitric

332    oxide synthase (eNOS) can be found in erythrocytes, where parasite-arginine  
333    deprivation decreases deformability of these cells as a result of reduced NO  
334    production (Cobbold et al., 2016). Here we show that upon ablation of *Slc7a7* in all  
335    cells, erythrocytes present reduced mean corpuscular volume and mean corpuscular  
336    hemoglobin, which has also been also described in LPI patients (Al-Qattan et al.,  
337    2021). Since arginine is the metabolite recovered by citrulline administration, we  
338    hypothesized that hypoargininemia plays a key role in erythropoiesis and RBC size.  
339    Altered RBCs in *Slc7a7*<sup>-/-</sup> leads to increased erythrophagocytosis. Furthermore, bone  
340    marrow-derived macrophages from  $\gamma^+$ LAT1 knock out mice did not show an increased  
341    rate of erythrophagocytosis when exposed to control erythrocytes, further supporting  
342    that the observed abnormalities in *Slc7a7*<sup>-/-</sup> RPMs (i.e. increased markers of  
343    erythrophagocytosis) are primed by altered erythrocytes rather than by a cell-  
344    autonomous defect of RPMs.  
345    RPMs prime erythrocyte degradation and iron recycling, and defects in numerous  
346    pathways can lead to iron overload in macrophages (Knutson et al., 2005). Such  
347    pathological conditions can thus lead to compromised iron metabolism and have an  
348    impact on macrophages (Ganz, 2012; Soares and Hamza, 2016). For instance, aged  
349    or damaged erythrocytes can express “eat me” signals and acutely trigger the  
350    erythrophagocytosis machinery (Luo et al., 2016; Oldenborg, 2000; Park and Kim,  
351    2017) subsequently causing iron accumulation in RPMs (Dichtl et al., 2018) as we  
352    clearly observed in the *Slc7a7*<sup>-/-</sup> model. We postulate therefore that defective arginine  
353    availability is also at the basis of iron accumulation because citrulline administration  
354    recovers normal iron levels in liver, spleen and BM, and they are also not present in  
355    *Slc7a7*<sup>LysM</sup> tissues.

356 FPN1 is the only known iron exporter involved in iron efflux in macrophages.  
357 Mechanistically, FPN1 is regulated at the protein level by hepcidin, which mediates its  
358 degradation (Drakesmith et al., 2015). In this regard, the increased hepatic iron  
359 content and ferritin levels (Nemeth and Ganz, 2009) would be at the root of induced  
360 hepcidin expression as depicted by increased *BMP6* liver mRNA expression. As a  
361 consequence of increased plasma hepcidin, *Slc7a7<sup>-/-</sup>* show decreased FPN1  
362 expression in RPMs, which was further confirmed by both flow cytometry and western  
363 blot analysis. Presumably, in this LPI mouse model the dysfunctional RBC generation  
364 increases erythrophagocytosis by a mechanism that, at the same time, leads to  
365 overwork of the fewer RPMs and disrupted iron handling by altered FPN1  
366 homeostasis.

367 Erythroblast differentiation is orchestrated mainly by EPO expression (Jelkmann,  
368 2011; Moritz et al., 1997). Our findings that *Slc7a7<sup>-/-</sup>* mice show reduced EPO in  
369 circulation, highlights the importance of *Slc7a7*-mediated systemic arginine  
370 availability. However, while BM transplant failed to rescue the hematological  
371 alterations, it did recover macrophage iron accumulation, suggesting thus two additive  
372 mechanisms. On one hand defects in RBC maturation are caused by an unbalanced  
373 systemic metabolic environment rather than by a cell-autonomous defect. On the  
374 other hand, macrophage iron accumulation also requires *Slc7a7* ablation in  
375 macrophages. Future work is needed to elucidate the link between *Slc7a7*-mediated  
376 systemic arginine availability and EPO production, and between macrophage y<sup>+</sup>LAT1  
377 and FPN1 expression.

378 Substantial advances in the research field of LPI have been scarce during the last  
379 decade, which can be probably explained by the huge phenotypic variability found  
380 among LPI patients (Al-Qattan et al., 2021; Ogier de Baulny et al., 2012; Posey et al.,

381 2014). In a previous work we showed that the inducible total *Slc7a7*<sup>-/-</sup> mouse model  
382 recapitulates the main hallmarks of the human LPI complications, such as  
383 hypoargininemia, hyperammonemia and PAP (Bodoy et al., 2019; Ogier de Baulny et  
384 al., 2012; Parto et al., 1994). In the current work we show that *Slc7a7*<sup>-/-</sup> mouse model  
385 has increased erytrophagocytosis, elevated serum ferritin, altered hemogram and  
386 abnormal iron retention in macrophages (Ogier de Baulny et al., 2012). Moreover, the  
387 systemic metabolic condition of LPI is an essential driver for the hematologic  
388 complications. In addition, *Slc7a7*<sup>-/-</sup> mice showed deficient erythropoiesis, a trait that  
389 parallels the reduced number of reticulocytes in some LPI patients, an alteration that  
390 has not been fully explored (Al-Qattan et al., 2021). Our results shifted the spotlight of  
391 increased erytrophagocytosis by abnormally functioning macrophages to altered  
392 erythrocytes.

393 Historically, systemic metabolic condition and immune-hematologic complications of  
394 LPI have been considered as independent entities, such is the case that some authors  
395 concerned about a potential detrimental effect of citrulline treatment in the  
396 development of immune complications (Ogier de Baulny et al., 2012). Nevertheless,  
397 more recently low argininemia was revealed as a poor prognosis factor in LPI (Mauhin  
398 et al., 2017). Now, our work upholds the premise that the handling of the metabolic  
399 derangements could prove beneficial not only for the metabolic hallmarks of the  
400 diseases but also for the reported hematologic complications of the patients.

401

## 402 **Author Contributions**

403 F.S., J.G., and S.B. designed and performed experiments, interpreted and analyzed  
404 data. J.G., S.B., and M.P. designed research and wrote the manuscript with input from

405 all of the authors. J.C. performed research. G.W and M.S. provided reagents and  
406 provided intellectual input. A.O., R.A. and A.Z. provided reagents.

407 The authors declare no competing financial interests.

408 Correspondence: Susanna Bodoy, Institute for Research in Biomedicine Barcelona,  
409 Baldiri Reixac, 12, Barcelona 08028, Spain; e-mail:  
410 [susanna.bodoy@irbbarcelona.org](mailto:susanna.bodoy@irbbarcelona.org); Manuel Palacín, Institute for Research in  
411 Biomedicine Barcelona, Baldiri Reixac, 12, Barcelona 08028, Spain; e-mail:  
412 [manuel.palacin@irbbarcelona.org](mailto:manuel.palacin@irbbarcelona.org).

413 **Acknowledgements**

414 This work was supported by grants from the Spanish Ministry of Science and  
415 Innovation (grant SAF2015-64869-R-FEDER and RTI2018-094211-B-100), Ramon  
416 Areces Fundation (I.O.F.R.ARECES) and the Generalitat de Catalunya (grant 2017  
417 SGR 961). Grant RTI2018-101735-B-I00 from the Spanish Ministry of Science and  
418 Innovation to MS. The EMBO Short Term Fellowship Program facilitated the  
419 collaboration between international groups. We are also grateful to Dr. Angel Nebreda  
420 at the IRB Barcelona, Spain, for *LysM-Cre* transgenic mice; Dra Anna Bigas from  
421 IMIM, Spain, for CD45.1 mice. We thank Jorge Seco and Vanessa Hernández for  
422 technical assistance and help with the experimental animals, and the Daniel Bravo  
423 Foundation for support with amino acid determination.

424

425

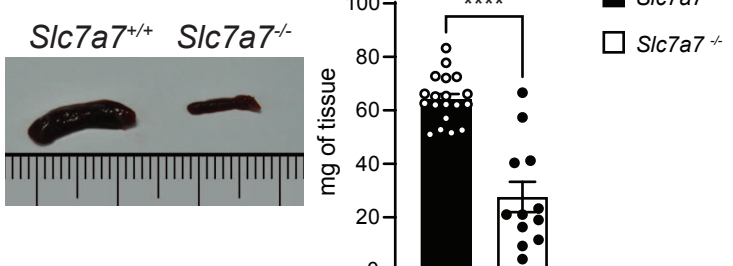
426

427

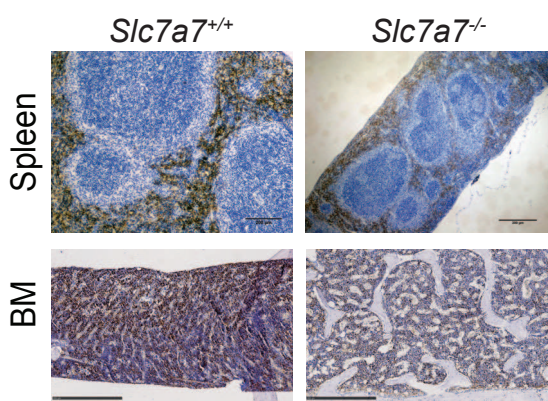
428

429

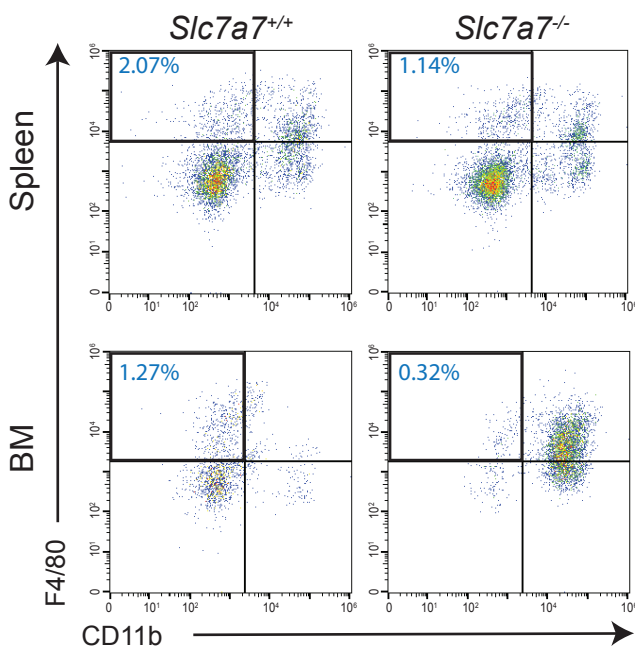
**A**



**B**

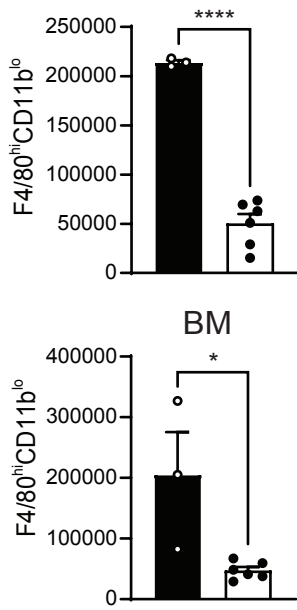


**C**

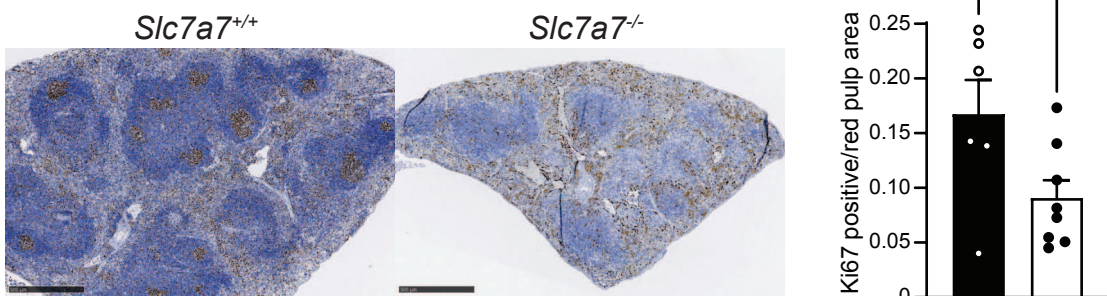


Spleen

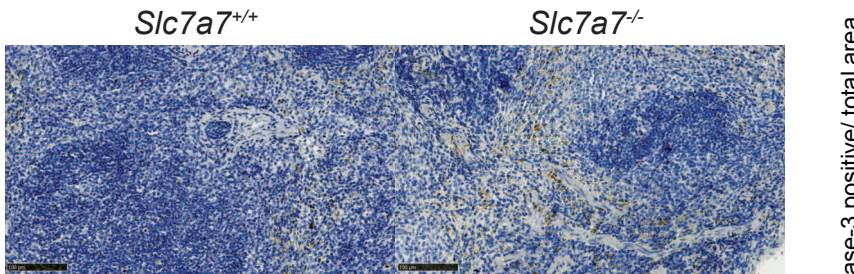
Monocytes



**E**



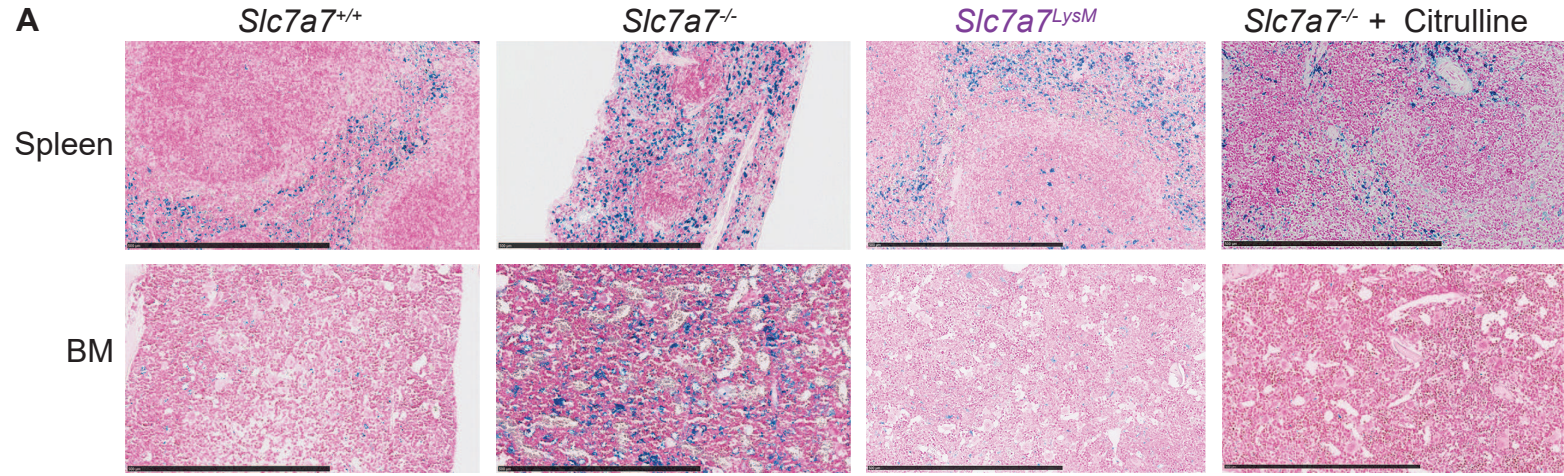
**F**



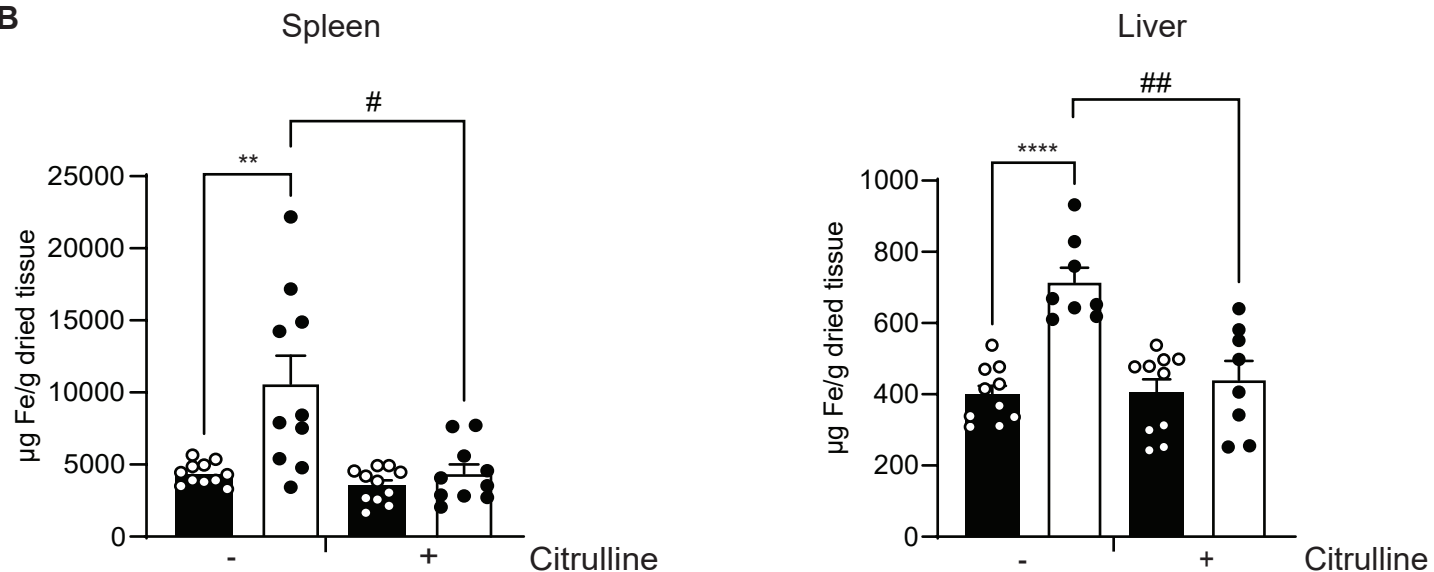
Caspase-3

430 **Figure 1.  $y^t$ LAT1 conditional knockout mice present a drastic reduction of BMMs**  
431 **and RPMs.** (A) *Slc7a7<sup>-/-</sup>* mice and its control littermates were dissected, and spleens  
432 were photographed (left panel). Spleen weights are indicated on the right panel. (B)  
433 Representative immunohistochemistry staining of F4/80<sup>+</sup> cells in the spleen and bone  
434 marrow (BM) from *Slc7a7<sup>+/+</sup>* and *Slc7a7<sup>-/-</sup>* animals. Spleen scale bar, 200  $\mu$ m, bone  
435 marrow scale bar, 500  $\mu$ m. (C) Flow cytometry quantification of total number of red  
436 pulp macrophages per spleen and bone marrow macrophages per femur and tibia  
437 (CD11b<sup>lo</sup>, F4/80<sup>hi</sup>). (D) Comparison of peripheral blood concentration of circulating  
438 monocytes levels. (E) Representative Ki67 staining of spleen of *Slc7a7<sup>+/+</sup>* and *Slc7a7<sup>-/-</sup>*  
439 mice (left) and its quantification (right). Scale bar, 500  $\mu$ m. (F) Representative Active  
440 Caspase-3 staining of spleen of *Slc7a7<sup>+/+</sup>* and *Slc7a7<sup>-/-</sup>* mice (left) and its quantification  
441 (right). Scale bar, 100  $\mu$ m. Data are mean  $\pm$  SEM. \*  $P \leq 0.05$ , \*\*\*  $P \leq 0.001$ , \*\*\*\*  $P \leq$   
442 0.0001 between genotypes.  $P$  values were calculated using two-tailed *t*-test.  
443  
444  
445  
446  
447  
448  
449  
450  
451  
452  
453

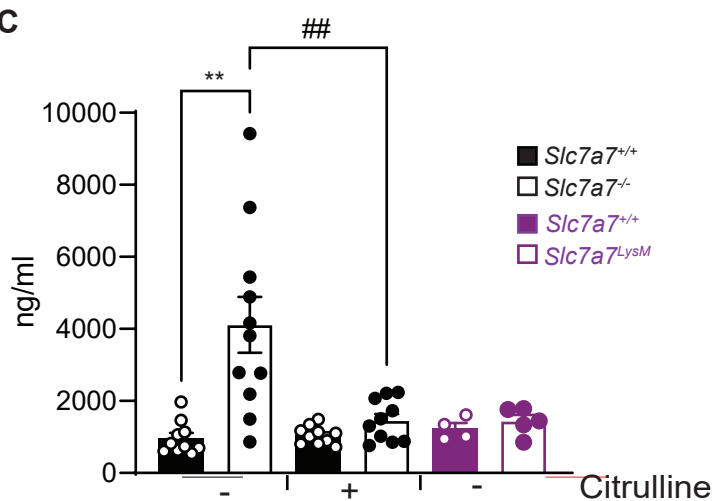
**A**



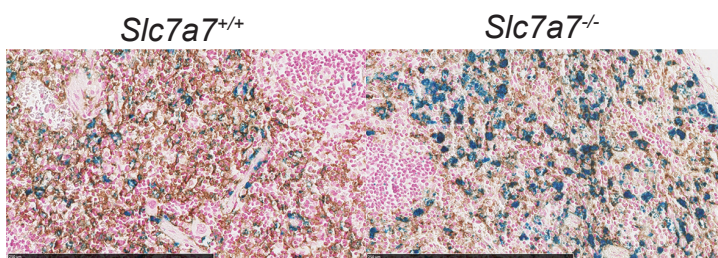
**B**



**C**



**D**



454 **Figure 2. *Slc7a7*  $^{/-}$  RPMs show increased iron accumulation and exacerbated**  
455 **iron metabolism.** (A) Representative iron Perl's Prussian Blue staining of spleens and  
456 bone marrow (BM) from indicated genotype supplemented or not with citrulline (1 g/L  
457 of drinking water). Scale bars, 500  $\mu$ m. (B) Total non-heme iron content from spleen  
458 (left panel) and liver (right panel) from *Slc7a7*<sup>+/+</sup> and *Slc7a7*<sup>/-</sup> mice. (C) Plasma ferritin  
459 quantification of indicated genotype supplemented or not with citrulline. (D) F4/80  
460 (brown) and iron (blue) staining of spleen sections of indicated genotype. Scale bar,  
461 250  $\mu$ m. Data are mean  $\pm$  SEM. \*\*  $P \leq 0.01$ , \*\*\*  $P \leq 0.001$  between genotypes. #  $P \leq$   
462 0.05, ##  $P \leq 0.01$  vs. *Slc7a7*<sup>/-</sup> mice without citrulline.  $P$  and # values were calculated  
463 using two-tailed *t*-test.

464

465

466

467

468

469

470

471

472

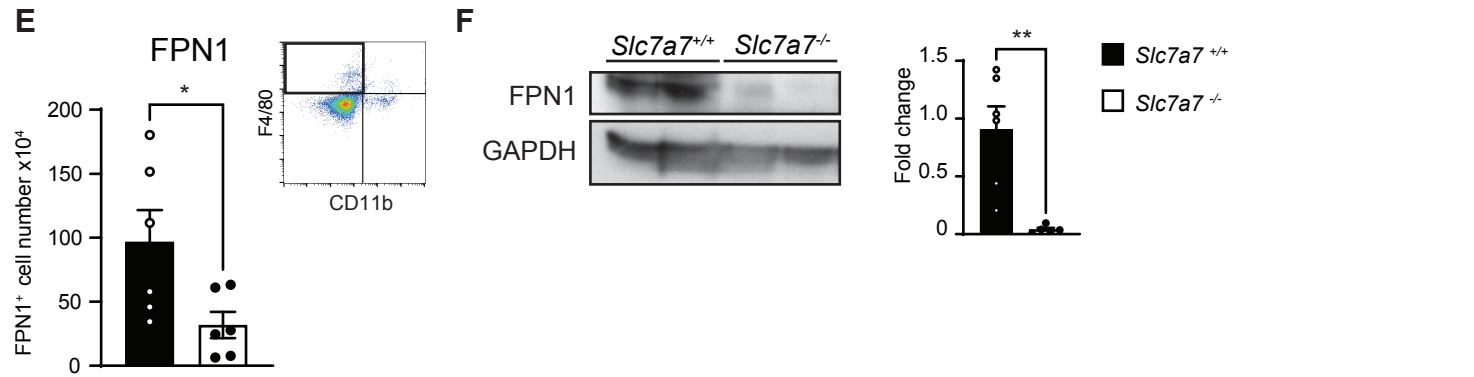
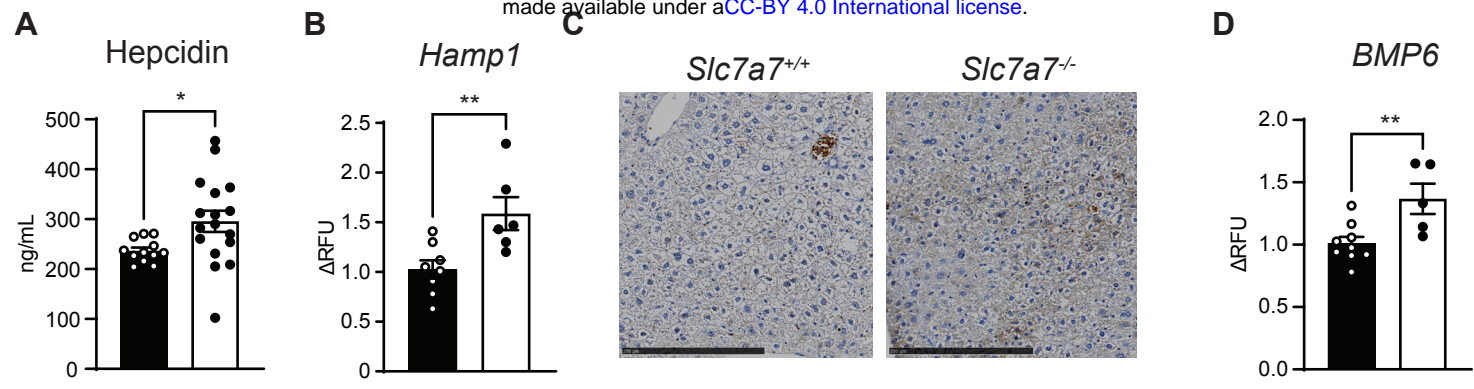
473

474

475

476

477



478 **Figure 3. Total loss of *Slc7a7* results in decreased FPN1 expression.** (A) Plasma  
479 hepcidin levels in *Slc7a7<sup>+/+</sup>* and *Slc7a7<sup>-/-</sup>* mice. (B) *Hamp1* mRNA levels (i.e., gene  
480 encoding for hepcidin) of *Slc7a7<sup>+/+</sup>* and *Slc7a7<sup>-/-</sup>* mice livers. (C) Iron histology by  
481 enhanced Pearl's Prussian blue (brown) staining of liver sections of indicated  
482 genotype. Scale bar, 250  $\mu$ m. (D) *BMP6* mRNA expression of *Slc7a7<sup>+/+</sup>* and *Slc7a7<sup>-/-</sup>*  
483 mice livers. (E) Absolute cell number of CD11b<sup>lo</sup>, F4/80<sup>hi</sup>, FPN1<sup>hi</sup> per spleen and  
484 representative FACS plot showing selected gate. (F) FPN1 protein expression in  
485 spleen membranes of the indicated genotypes. Quantification is expressed as  
486 FPN1/GAPDH fold change. Data are represented as mean  $\pm$  SEM. \*  $P \leq 0.05$ , \*\*  $P \leq$   
487 0.01 between genotypes.  $P$  values were calculated using two-tailed *t*-test.

488

489

490

491

492

493

494

495

496

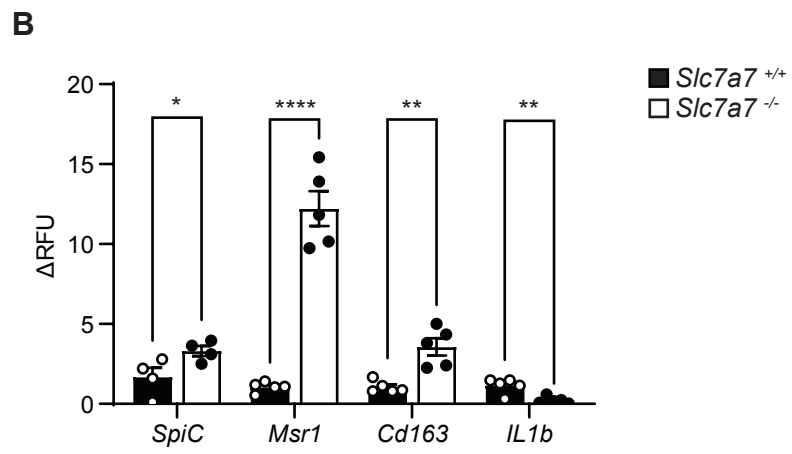
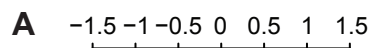
497

498

499

500

501



**C** Bone Marrow Derived Macrophages



502 **Figure 4.  $y^+$ LAT1 ablation leads to increased erythrophagocytosis.** (A) RPMs  
503 ( $F4/80^{hi}CD11b^{lo}$ ) were sorted and gene expression analysis was carried out using the  
504 Affymetrix platform and a selection of RPM-associated genes(Haldar et al., 2014;  
505 Kohyama et al., 2009) was plotted as a heat map. Black boxes indicate the *Slc7a7<sup>+/+</sup>*  
506 genotype and empty boxes the *Slc7a7<sup>-/-</sup>* genotype. (B) Quantitative RT-PCR analysis  
507 of mRNA expression levels of indicated genes related to erythrophagocytosis and  
508 differentiation in RPM of *Slc7a7<sup>+/+</sup>* and *Slc7a7<sup>-/-</sup>* mice. (C) Erythrophagocytosis assay.  
509 Briefly, BMDMs were co-incubated with previously labelled erythrocytes. *Slc7a7<sup>+/+</sup>*  
510 erythrocytes (blue circles) were labelled with CellVue Claret, while *Slc7a7<sup>-/-</sup>*  
511 erythrocytes (orange circles) were labelled with PKH26. Left: Representative dot plots  
512 show the gating strategy for the erythrophagocytosis assay. Right: Percentage of the  
513 cell populations analyzed. Filled bars and empty bars represent *Slc7a7<sup>+/+</sup>* and *Slc7a7<sup>-/-</sup>*  
514 macrophages, respectively. Data are mean  $\pm$  SEM. \*  $P \leq 0.05$ , \*\*  $P \leq 0.01$ , \*\*\*  $P \leq$   
515 0.001, \*\*\*\*  $P \leq 0.0001$  between genotypes.  $P$  values were calculated using two-tailed  
516 *t*-test.

517

518

519

520

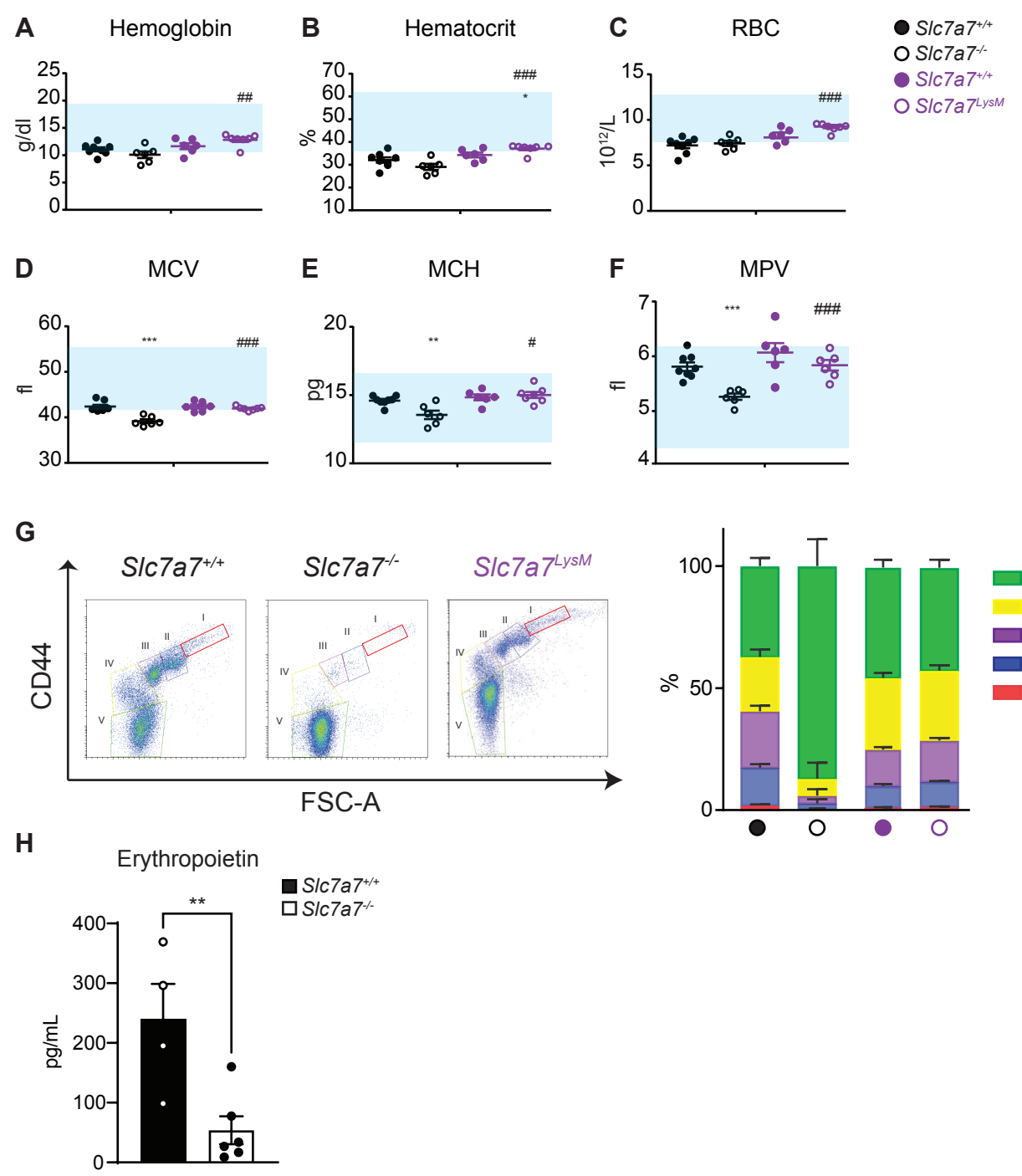
521

522

523

524

525

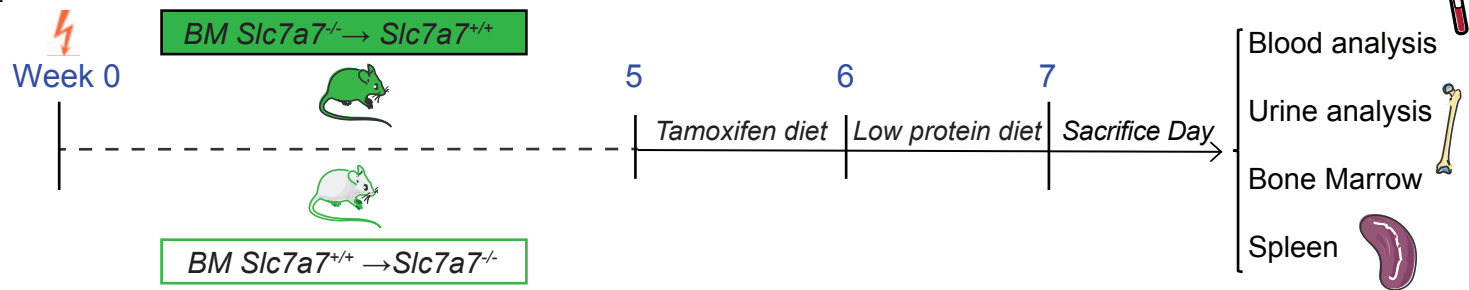


526 **Figure 5.  $y^+$ LAT1 depletion results in defective erythropoiesis. (A-F)**  
527 Quantification of blood hemoglobin (A), hematocrit (B), RBC concentration (C), mean  
528 corpuscular volume (D), mean corpuscular hemoglobin (E) and mean platelet volume  
529 (F) of indicated genotype. (G) Left: Representative dot plots show the gating strategy  
530 for erythroid progenitors (V, IV, III, II and I) (Chen et al., 2009) from indicated genotype.  
531 Briefly, cells were first gated in TER119<sup>+</sup> and further separated by CD44 versus  
532 Forward Scatter (FSC-A). Right: Percentage of the cell populations analyzed. (H)  
533 Plasma erythropoietin levels in *S/c7a7<sup>+/+</sup>* and *S/c7a7<sup>-/-</sup>* mice fed with a low protein diet.  
534 Data are mean  $\pm$  SEM. All experiments were performed independently at least twice.  
535 \*  $P \leq 0.05$ , \*\*  $P \leq 0.01$ , \*\*\*  $P \leq 0.001$  between genotypes.  $P$  values were calculated  
536 using two-tailed *t*-test.

537  
538  
539  
540  
541  
542  
543  
544  
545  
546  
547  
548  
549

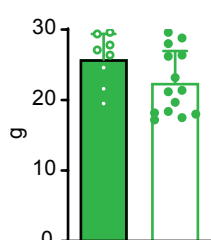


**A**



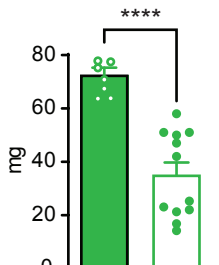
**B**

Body weight



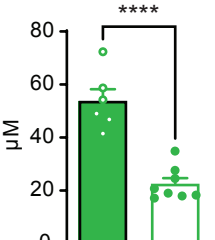
**C**

Spleen



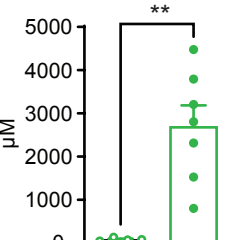
**D**

Arginine



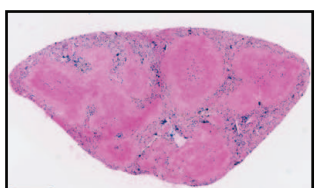
**E**

Orotic Acid

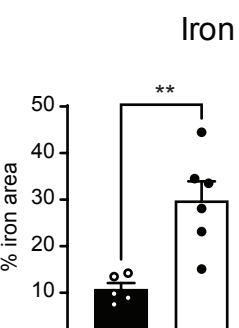
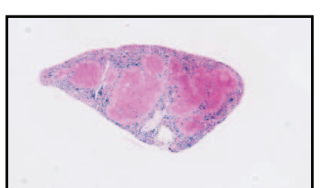


**F**

**BM *Slc7a7*<sup>-/-</sup> → *Slc7a7*<sup>+/+</sup>**

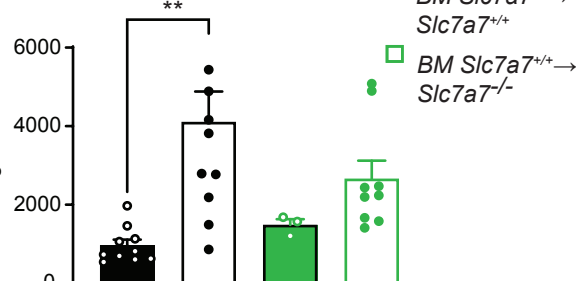


**BM *Slc7a7*<sup>+/+</sup> → *Slc7a7*<sup>-/-</sup>**



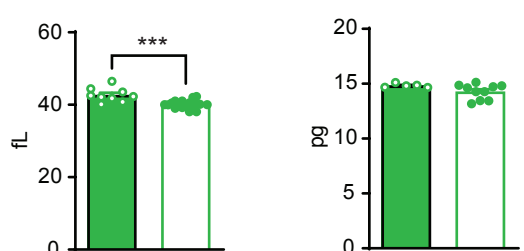
**G**

Ferritin

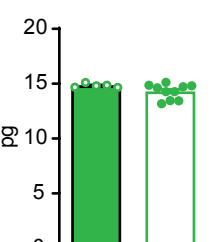


**H**

MCV

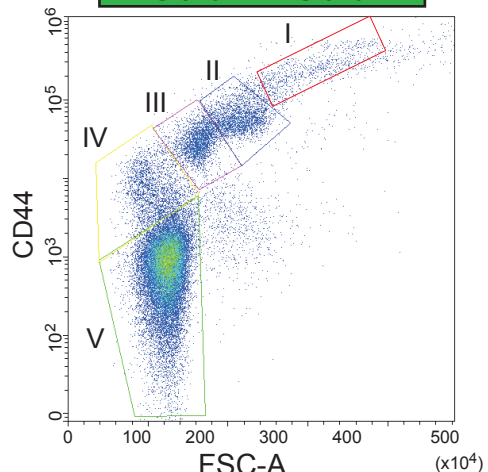


MCH

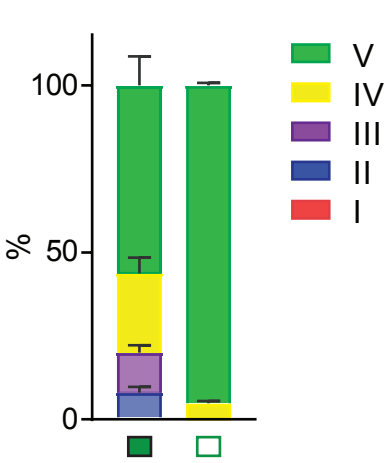
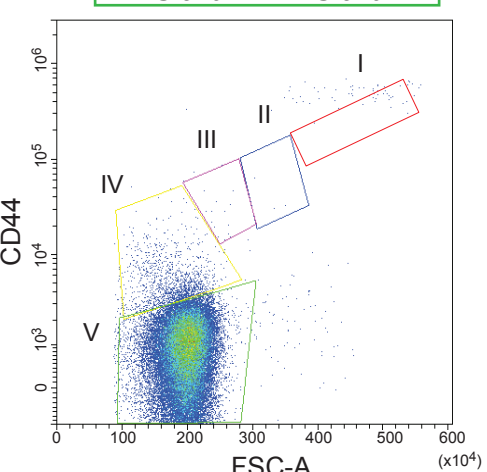


**J**

**BM *Slc7a7*<sup>-/-</sup> → *Slc7a7*<sup>+/+</sup>**



**BM *Slc7a7*<sup>+/+</sup> → *Slc7a7*<sup>-/-</sup>**



550 **Figure 6. Iron accumulation but not defective hematopoiesis and metabolic**  
551 **derangement improves after bone-marrow transplant.** (A) 5 weeks after transplant,  
552 mice were first fed a tamoxifen diet for 1 week and then a low-protein diet for 10 days  
553 prior to sacrifice day. (B-E) Body weight (B), spleen weight (C), plasma arginine (D),  
554 and urine orotic acid (E) of *Slc7a7<sup>-/-</sup>* mice transplanted with wild-type CD45.2 bone  
555 marrow (BM *Slc7a7<sup>+/+</sup>* → *Slc7a7<sup>-/-</sup>*) and *Slc7a7<sup>+/+</sup>* mice transplanted with *Slc7a7<sup>-/-</sup>*  
556 CD45.1 bone marrow (BM *Slc7a7<sup>-/-</sup>* → *Slc7a7<sup>+/+</sup>*). (F) Left: Isolated spleens of the  
557 indicated genotypes were embedded in paraffin for histopathological examination  
558 (Perl's Prussian Blue). Scale bar, 500 μm. Right: Percentage of iron area in the  
559 indicated genotypes and transplanted mice. (G) Plasma ferritin levels in *Slc7a7<sup>+/+</sup>* and  
560 *Slc7a7<sup>-/-</sup>* mice, and *Slc7a7<sup>-/-</sup>* and *Slc7a7<sup>+/+</sup>* mice transplanted with wild-type BM and  
561 *Slc7a7<sup>-/-</sup>* BM, respectively. (H-I) Hematological analysis (MCV, mean corpuscular  
562 volume; MCH, mean corpuscular hemoglobin) of *Slc7a7<sup>-/-</sup>* mice transplanted with wild-  
563 type CD45.2 bone marrow and *Slc7a7<sup>+/+</sup>* mice transplanted with *Slc7a7<sup>-/-</sup>* CD45.1 bone  
564 marrow. (J) Left: Representative dot plots show the gating strategy for erythroid  
565 progenitors (V, IV, III, II and I) (Chen et al., 2009) of *Slc7a7<sup>-/-</sup>* mice transplanted with  
566 wild-type BM and *Slc7a7<sup>+/+</sup>* mice transplanted with *Slc7a7<sup>-/-</sup>* bone marrow. Left: Boxes  
567 in the flow cytometry plots represents I-IV erythroblasts populations. Right: Percentage  
568 of the cell populations analyzed. Data are mean ± SEM. All experiments were  
569 performed independently at least twice. \*  $P \leq 0.05$ , \*\*  $P \leq 0.01$ , \*\*\*  $P \leq 0.001$ , \*\*\*\*  $P \leq$   
570 0.0001 between genotypes.  $P$  values were calculated using two-tailed *t*-test.

571

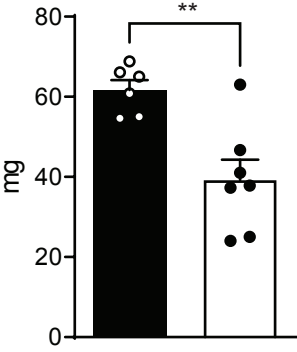
572

573

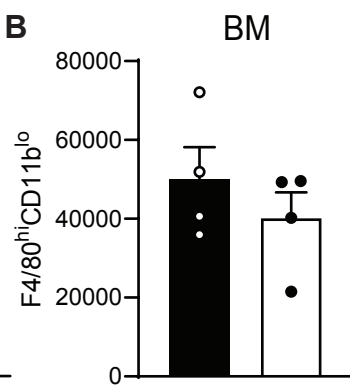
574

## Supplementary Figure 1

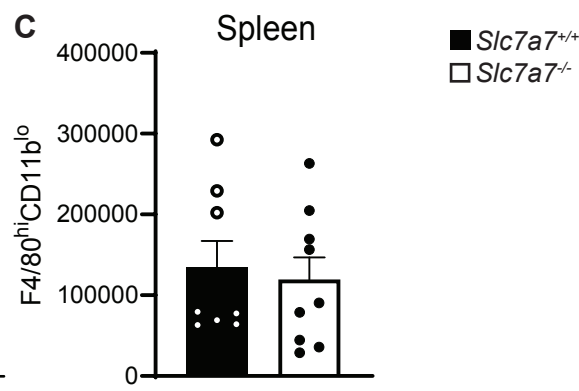
**A**



**B**



**C**



575 **Supplementary Figure 1. *Slc7a7*<sup>-/-</sup> mouse model treated with citrulline improve**  
576 **spleen weight and recover BMMs and RPMs number. (A)** *Slc7a7*<sup>-/-</sup> mice and its  
577 control littermates treated with citrulline in the drinking water (1g/L) were dissected,  
578 and spleens were photographed (left panel). Spleen weights are indicated on the right  
579 panel. (B) Flow cytometry quantification of total number of bone marrow (BM)  
580 macrophages and red pulp macrophages (C) per femur and tibia (CD11b<sup>lo</sup>, F4/80<sup>hi</sup>).  
581 Data are mean  $\pm$  SEM. \*\* $P \leq 0.01$  between genotypes.  $P$  values were calculated using  
582 two-tailed *t*-test.

583

584

585

586

587

588

589

590

591

592

593

594

595

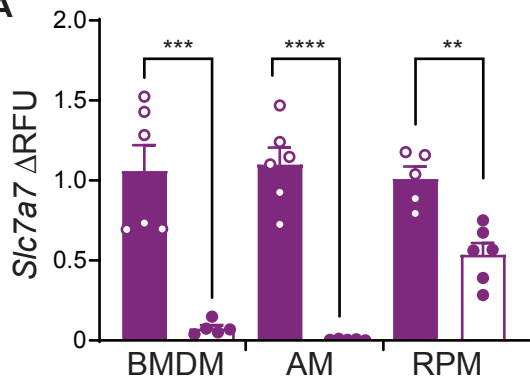
596

597

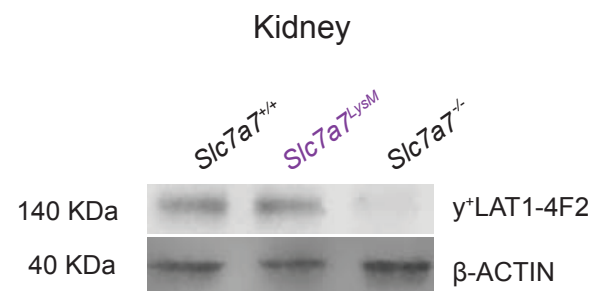
598

## Supplementary Figure 2

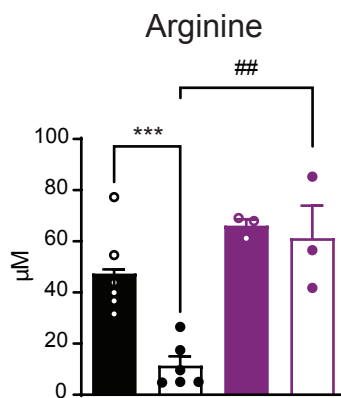
**A**



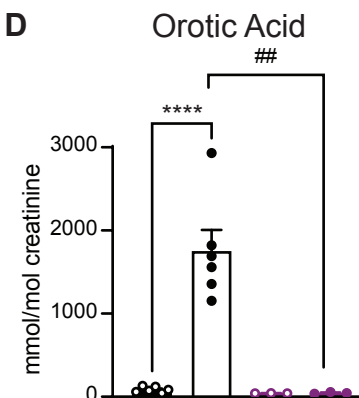
**B**



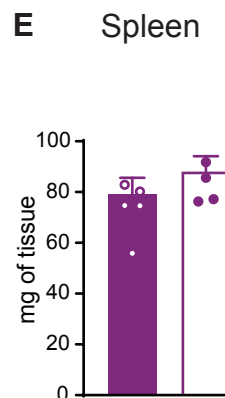
**C**



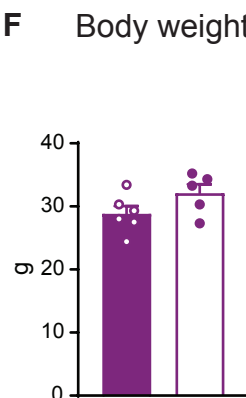
**D**



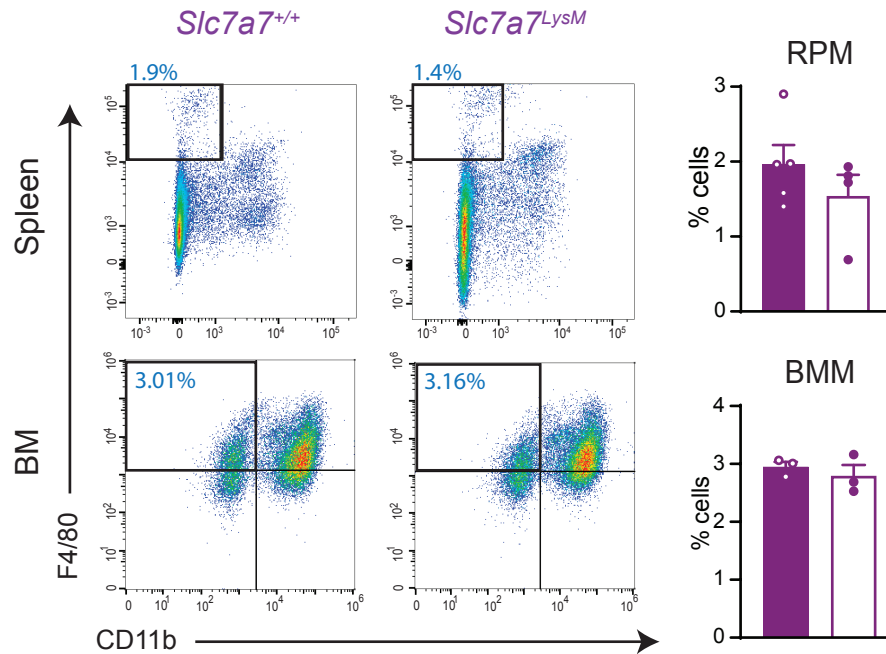
**E**



**F**



**G**



599 **Supplementary Figure 2.  $y^+$ LAT1 deficiency in myeloid cell line does not**  
600 **reproduce the deficiencies of the conditional knockout mouse.** (A) mRNA  
601 expression of *Slc7a7* gene in BMDMs, AMs and RPMs from *Slc7a7*<sup>LysM-/-</sup> and their  
602 control. (B)  $y^+$ LAT1 protein expression of kidney membranes in the indicated  
603 genotypes. (C) Plasma arginine, (D) urine orotic acid, (E) spleen and (F) body weight  
604 of *Slc7a7*<sup>+/+</sup>, *Slc7a7*<sup>-/-</sup>, *Slc7a7*<sup>LysM-/-</sup> mice and their control counterparts. (G) Flow  
605 cytometry analysis with the indicated markers on BMs and splenocytes of the  
606 designated genotypes. The percentage of CD11b<sup>lo</sup>F4/80<sup>hi</sup> is shown (right panel). Data  
607 are mean  $\pm$  SEM. \*\*  $P \leq 0.01$ , \*\*\*  $P \leq 0.001$  between genotypes. #  $P \leq 0.05$ , ##  $P \leq 0.01$   
608 vs. *Slc7a7*<sup>-/-</sup> mice.  $P$  values were calculated using two-tailed *t*-test.

609

610

611

612

613

614

615

616

617

618

619

620

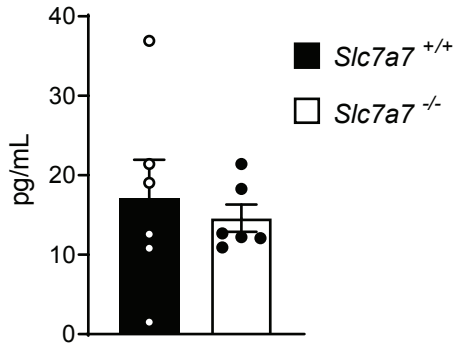
621

622

623

**Supplementary Figure 3**

**A**



**B**

	<b>Hallmark Term</b>	<b>PValue</b>	<b>NES</b>
	UV response DN	0.001	2.584
	Xenobiotic metabolism	0.044	2.025
	Complement	0.026	1.883
	Wnt-β catenin signaling	0.012	1.855
	Protein secretion	0.043	1.624
	G2M checkpoint	0	-3.917
	IL2 STAT5 signaling	0	-3.311
	Mitotic spindle	0	-3.07
	Inflammatory response	0	-3.049
	IL6 JAK STAT3 signaling	0	-2.797
	TNF-α signaling via NFKB	0.001	-2.599
	Interferon γ response	0.001	-2.584
	Allograft rejection	0	-2.569
	Estrogen response late	0.007	-2.518
	KRAS signaling up	0.007	-2.509
	E2F Targets	0	-2.469
	Angiogenesis	0.005	-2.263
	Apoptosis	0	-2.132
	Apical Junction	0.009	-2.13
	Unfolded protein response	0.009	-2.099
	Estrogen response early	0.017	-1.981
	Glycolysis	0.054	-1.975
	mTORC1 SIGNALING	0.033	-1.913
	P53 Pathway	0.094	-1.637
	Fatty acid metabolism	0.131	-1.557
	Heme metabolism	0.187	-1.412

624 **Supplementary Figure 3. IL6 plasma levels and broad hallmarks pathways**

625 (A) Plasma IL6 levels of *Slc7a7<sup>+/+</sup>* and *Slc7a7<sup>-/-</sup>* mice. Data are mean  $\pm$  SEM. *P* values  
626 were calculated using two-tailed *t*-test. (B) The most significative pathways in *Slc7a7<sup>-/-</sup>*  
627 red pulp macrophages, Pvalue and Normalized Enrichment Score (NES) values are  
628 shown.

629

630

631

632

633

634

635

636

637

638

639

640

641

642

643

644

645

646

647

648

649 **MATERIALS AND METHODS**

650 ***Data and code availability***

651 Microarray data has been deposited in a public repository and the accession  
652 numbers is GSE164827.

653 ***Animals***

654 All animal work was approved and conducted according to guidelines established. This  
655 project (DARP n°9177) has been assessed favourably by the Institutional Animal Care  
656 and Use Committee from Parc Científic de Barcelona (IACUC-PCB) and the IACUC  
657 considers that the above-mentioned project complies with standard ethical regulations  
658 and meets the requirements of current applicable legislation (RD 53/2013 Council  
659 Directive; 2010/63/UE; Order 214/1997/GC). C57BL/6 mice were purchased from  
660 Harlan Europe. *Slc7a7*<sup>loxP/loxP</sup> mice were generated by Eurogentec. To generate  
661 *Slc7a7*<sup>-/-</sup> and *Slc7a7*<sup>LysM</sup> mice, *Slc7a7*<sup>loxP/loxP</sup> were crossed with UBC-Cre-ERT2 mice  
662 from The Jackson Laboratory and LysM-Cre provided by Dr. Ángel R. Nebreda,  
663 respectively. Male or female mice of 12 weeks old were used. Mice were housed in  
664 groups of 2-5 animals per cage and were kept under a 12 h dark-light period. Food  
665 and water were supplied *ad libitum*. Animals were fed a standard diet (Teklad global  
666 14% protein rodent maintenance diet) until tamoxifen induction, which consisted of a  
667 tamoxifen diet for one week. After the induction period, animals were kept on a low-  
668 protein diet for 7-10 days, supplemented or not with 1g/l L-citrulline in drinking water.  
669 Control and *Slc7a7*<sup>-/-</sup> littermates on a C57Bl6/J genetic background were sacrificed at  
670 10-12 weeks of age by cervical dislocation. Tissues were dissected and flash-frozen  
671 in liquid nitrogen for RNA, protein, and iron quantification studies. For histological  
672 analysis, mice were anesthetized with ketamine and xylazin (respectively 1 mg and  
673 0.1 mg per 10 g of body weight, i.p., respectively) and subjected to transcranial

674 perfusion. For hematological and biochemical studies, EDTA or heparin blood was  
675 collected from cardiac puncture. Bone marrow was flushed out from femur and tibia  
676 bones.

677 Mice carrying the myeloid-specific knockout of the *Slc7a7* gene (*LysM*<sup>Cre/+</sup>  
678 *Slc7a7*<sup>fl/fl</sup>) were sacrificed at 12 weeks of age, and only those with more than 80%  
679 deletion of endogenous protein were used for the experiments.

#### 680 **Bone marrow transplantation (BMT)**

681 Recipient mice were lethally irradiated (9.5Gy) and transplanted with 2x10<sup>6</sup> bone  
682 marrow (BM) cells by retro-orbital injection (Bennett et al., 2018). For the re-population  
683 experiments, total BM cells from either *Slc7a7*<sup>-/-</sup> (CD45.2) or *Slc7a7*<sup>+/+</sup> (CD45.1) mice  
684 were transplanted into lethally irradiated B6 recipient mice (CD45.1 or CD45.2). As a  
685 follow-up step, five weeks after transplantation to allow whole body hematopoiesis  
686 regeneration, mice were subjected to tamoxifen diet for 7 days, and then treated with  
687 a low-protein diet for 10 days prior to the sacrifice. BM reconstitution was monitored  
688 by flow cytometry.

689  $\gamma$ -Irradiation of mice was performed in a 137Cs- $\gamma$  IBL 437C H irradiator (Shering CIS  
690 bio international) at 2.56Gy/min rate for the indicated dosage. The irradiated mice were  
691 inspected daily. Mice were given *Baytril* water containing antibiotics (Bayer, Shawnee  
692 Mission, JS) for at least 30 days to reduce the probability of infection from opportunistic  
693 pathogens.

#### 694 **Flow cytometry and cell sorting**

695 For the analysis of splenocytes and bone marrow cells, crushed spleens and flushed  
696 BM were isolated and incubated with Fc block (anti-mouse CD16/32; Thermofisher)  
697 for 30 min on ice. Cell suspensions were stained for the expression of CD71; CD11b;  
698 CD45.1; CD45.2 (BD Biosciences); CD34 (eBiosciences); F4/80; TER119; CD106

699 (BioLegend) for 30 min on ice. Flow cytometry analysis was performed on Gallios (BD  
700 Boisces). For spleen staining, crushed tissues were filtered through a 40  $\mu$ M cell  
701 strainer and erythroid cells were removed by incubation with ammonium-chloride-  
702 potassium lysis buffer prior to Fc blocking. Cell sorting (purity > 90%) was carried out  
703 using a FACS Aria II (BD Biosciences). For microarray analysis, spleens were  
704 prepared as described above and stained with anti-CD106, anti-CD11b and anti-F4/80  
705 (ThermoFisher) for purified RPMs.  
706 Cell doublets were excluded from all analyses and, when possible, dead cells were  
707 excluded by the use of DAPI. Data analysis was carried out using FlowJo<sup>TM</sup> Software.

708 ***In vitro erythrophagocytosis assay***

709 To prepare primary BMDMs, cells obtained from mouse femurs and tibia were cultured  
710 for 7 days in the presence of L-Cell (L929 SN) in DMEM supplemented with 10% FBS,  
711 penicillin (50 U/mL) and streptomycin (50  $\mu$ g/mL). BMDMs were plated 24 hours prior  
712 to the day of the experiment. On the day of the experiment, previously seeded BMDMs  
713 were activated with lipopolysaccharide (100 ng/mL) for 2h and fresh RBCs were  
714 extracted, washed and labelled with CellVue<sup>®</sup> or PKH26 following the manufacturer's  
715 instructions. RBCs were then incubated with previously activated BMDMs for 2  
716 minutes ( $10 \cdot 10^6$  RBC/ $1 \cdot 10^6$  BMDM) at 37°C in a 5% CO<sub>2</sub> incubator. Macrophages  
717 were washed twice with PBS and finally incubated with an erytholysis buffer (R&D  
718 Systems) to lyse non-ingested RBCs. Cells were then collected and analyzed by flow  
719 cytometry.

720 ***Histological sample preparation and analysis***

721 Samples were fixed overnight at 4°C with neutral buffered formalin. After fixation,  
722 bone tissue (femur) was washed with PBS 1x and decalcified with Osteosoft<sup>®</sup> reagent

723 for a minimum 15 days at RT. All samples were embedded in paraffin-  
724 embedded tissue sections (2-3  $\mu$ m in thickness) were air-dried and further dried at 60  
725 °C overnight. Bone sections were maintained at 60°C for 48 h.  
726 For special staining, paraffin-embedded tissue sections were dewaxed and stained  
727 with Iron Stain Kit to identify iron pigment using the Dako Autostainer Plus and  
728 following the manufacturer instructions. When combining Iron staining with F4/80 IHC,  
729 iron staining was done before following the described protocols.  
730 Prior to immunohistochemistry, sections were dewaxed and therefore epitope retrieval  
731 was performed using citrate buffer pH6 for 20 min at 121°C with an autoclave or  
732 proteinase K for 5 min at RT for anti-caspase 3 (Cell Signalling) and rat monoclonal  
733 Anti-F4/80 (eBioscience), respectively. For rabbit polyclonal anti-Ki67 (Abcam)  
734 sections were dewaxed as part of the antigen retrieval process using the low pH  
735 EnVision™ FLEX Target Retrieval Solutions (Dako, Burlington) for 20min at 97°C  
736 using a PT Link (Dako, Agilent). Quenching of endogenous peroxidase was performed  
737 by 10 min of incubation with Peroxidase-Blocking Solution at RT. Non-specific  
738 bindings were blocked using 5 % of goat normal serum or normal donkey serum mixed  
739 with 2.5 % BSA diluted in the wash buffer for 60 min at RT. The primary antibody  
740 dilutions used were 1:300, 1:100 and 1:2000, for 120 min, overnight or 60 min,  
741 respectively. The secondary antibody used was a BrightVision Poly-HRP-Anti Rabbit  
742 IgG Biotin-free, ready to use or the secondary antibody used was a Biotin-SP (long  
743 spacer) AffiniPure Donkey Anti-Rat IgG (H+L) at 1:500 (in wash buffer) for 60 min  
744 followed by amplification with Streptavidin-Peroxidase polymer at 1:1000. Antigen-  
745 antibody complexes were revealed with 3-3'-diaminobenzidine, with the same time  
746 exposure (1 min). Sections were counterstained with hematoxylin and mounted with

747 Mounting Medium, Toluene-Free using a Dako CoverStainer. Specificity of staining  
748 was confirmed with rabbit IgG, polyclonal - Isotype control or Normal Rat IgG Control.  
749 Image acquisition. Brightfield images were acquired with a NanoZoomer-2.0 HT  
750 C9600 digital scanner (Hamamatsu) equipped with a 20X objective. All images were  
751 visualized with the NDP.view 2 U123888-01 software. All images were visualized with  
752 a gamma correction set at 1.8 in the image control panel of the NDP.view 2 U12388-  
753 01 software.

754 Prior to immunohistochemistry, for Ki67 sections were dewaxed as part of the antigen  
755 retrieval process using the low pH EnVision™ FLEX Target Retrieval Solutions (Dako,  
756 Burlington) for 20 min at 97°C using a PT Link (Dako – Agilent). For caspase 3 samples  
757 were dewaxed and antigen retrieval treatment was performed with citrate buffer pH6  
758 for 20 min at 121°C with an autoclave. Quenching of endogenous peroxidase was  
759 performed by 10 min of incubation with Peroxidase-Blocking Solution (Dako REAL  
760 S2023). Rabbit polyclonal primary anti-Ki67 antibody (A. Menarini diagnostics – NCL-  
761 ki67p) was diluted 1:1000 with EnVision FLEX Antibody Diluent (K800621, Dako,  
762 Agilent) and incubated for 60 min at RT. The secondary antibody used was a  
763 BrightVision Poly-HRP-Anti Rabbit IgG Biotin-free, ready to use (Immunologic, DPVR-  
764 110HRP). Antigen–antibody complexes were revealed with 3-3'-diaminobenzidine,  
765 with the same time exposure per antibody (3 and 5 min respectively). Sections were  
766 counterstained with hematoxylin and mounted with Mounting Medium, Toluene-Free  
767 using a Dako CoverStainer.

768 ***Amino acid content***

769 Briefly, amino acids were determined by ion exchange chromatography with ninhydrin  
770 derivatization and spectrometric detection (Biochrom 30, Chromsystems, Cambridge,  
771 UK). Plasma (300 µL) were deproteinized with sulphosalicylic acid containing L-

772 norleucine as internal standard (final concentration 100  $\mu$ mol/L). After centrifugation,  
773 200  $\mu$ L of supernatant were adjusted to pH = 2.1 with lithium hydroxide, and then,  
774 injected onto the liquid chromatograph. Urinary orotic acid was analyzed following a  
775 spectrometric procedure (458 nm), by reacting with para-  
776 dimethylaminobenzaldehyde.

777 ***Tissue iron content***

778 Liver and spleen non-heme iron content was measured using the bathophenanthroline  
779 colorimetric method. Mouse tissues were dried at 45°C for 3 days, weighted, and  
780 digested for 48 h at 65°C in 10% TCA/10% HCl to allow deproteinization of non-heme  
781 iron. Diluted extracts were added to a 0.01% bathophenanthroline disulfonic acid,  
782 0.1% thioglycolic, 7M sodium acetate solution and the absorbance at 535 nm was  
783 measured using a spectrophotometer Ultrospec 3100pro (Amersham Biosciences).  
784 The iron content of samples was obtained by interpolation from a standard curve and  
785 calibrated to the weight of dried material (Jd and Th, 1968; Patel et al., 2002).

786 ***Plasma measurements***

787 ELISA kit was used to determine the IL6 (Abnova), hepcidin (Intrinsic Life Science),  
788 ferritin (Abcam) and erythropoietin (R&D Systems) proteins in fresh plasma. The  
789 procedures were done following the manufacturer's instructions.

790 ***Microarray analysis***

791 For gene expression analysis of RPMs, total RNA was isolated from previously purified  
792 cells using magnetic beads and the Agencourt RNA Clean XP kit (Beckman Coulter).  
793 Quality and quantity were assessed using a Bioanalyzer 2100 (Agilent Technologies,  
794 Palo Alto, CA). Library preparation and amplification were performed as described  
795 previously by (Gonzalez-Roca et al., 2010). RNA was amplified for 22 cycles and

796 purified using PureLink Quick PCR Purification kit (Invitrogen) in the Genomic Facility  
797 of IRB Barcelona.

798 ***Pre-processing of microarray data***

799 Microarray datasets were processed separately using R (R Core, 2019) packages affy  
800 (Gautier et al., 2004) and affyPLM (Bolstad et al., 2005) from Bioconductor  
801 (Gentleman et al., 2004). Raw cell files data were processed using RMA (Irizarry,  
802 2003) and annotated using the information available on the Affymetrix – ThermoFisher  
803 web page. Standard quality controls were performed in order to identify abnormal  
804 samples regarding: a) spatial artefacts in the hybridization process (scan images and  
805 pseudo-images from probe level models); b) intensity dependences of differences  
806 between chips (MVA plots); c) RNA quality (RNA digest plot); d) global intensity levels  
807 (boxplot of perfect match log-intensity distributions before and after normalization and  
808 RLE plots); and e) anomalous intensity profile compared to the rest of the samples  
809 (NUSE plots, Principal Component Analysis).

810 ***Differential expression***

811 A differential expression analysis was performed for *Slc7a7<sup>+/+</sup>* and *Slc7a7<sup>-/-</sup>*  
812 comparisons using a linear model with empirical shrinkage (Smyth, 2004) as  
813 implemented in Limma R package (Ritchie et al., 2015). This model included the batch  
814 of scanning for statistical control. Adjustment by multiple comparisons was performed  
815 using the Benjamini-Hochberg method (Benjamini and Hochberg, 1995).

816 ***Biological enrichment analysis***

817 Genes quantified in the microarray experiment were annotated according to the Broad  
818 Hallmark (Liberzon et al., 2015) gene sets collection. Broad Hallmark sets were

819 translated to mouse homologous genes using the R package biomaRt (Durinck et al.,  
820 2009).

821 Functional enrichment analyses were performed using a modification of ROAST (Wu  
822 et al., 2010), a rotation-based approach implemented in the R package limma (Ritchie  
823 et al., 2015) that is especially suitable for small size experiments. Such modifications  
824 were implemented to accommodate in the ROAST algorithm the statistical re-  
825 standardization proposed in (Efron and Tibshirani, 2007), which enables its use for  
826 competitive testing (Goeman and Bühlmann, 2007). The MaxMean (Efron and  
827 Tibshirani, 2007) statistic was used for testing geneset enrichment of Broad Hallmark.  
828 For each gene, the most variable probeset within each gene was used in these  
829 analyses (median absolute deviation).

830 The results of these analyses were adjusted by multiple comparisons using the  
831 Benjamini-Hochberg False Discovery Rate method (Benjamini and Hochberg, 1995).

832 ***Clustering and visualization***

833 Gene expression of selected genes was graphically represented in a heatmap with the  
834 heatmap R package, using a blue to red gradation, where red indicated the highest  
835 expression and blue corresponded to the lowest expression values. Previously, the  
836 expression data were summarized to the gene level using the most variable probeset  
837 mapping to the same gene (median absolute deviation), and expression values were  
838 centered and scaled gene-wise. Genes and samples were clustered using the Ward  
839 agglomeration method and the correlation and Euclidean distances, respectively. To  
840 gain clarity in the graphic, the most extreme values were truncated to -1.5 and 1.5.  
841 All analyses were carried out using R and Bioconductor.

842 ***RNA extraction and quantitative real-time PCR***

843 Mice were killed by cervical dislocation, and tissues were immediately frozen for RNA  
844 isolation. Total mRNA was extracted from BMDMs or AMs using the Rneasy Total  
845 RNA Isolation kit (Qiagen, Alameda, CA, USA), following the manufacturer's  
846 instructions. RNA concentrations were measured with Nanodrop ND-1000  
847 (ThermoFisher Scientific). Reverse transcription was performed with total RNA (2 ng)  
848 using the qScript cDNA SuperMix (Quantabio) following the manufacturer's  
849 instructions. PCRs were performed using the ABI Prism 7900 HT real-time PCR  
850 machine (Applied Biosystems, USA) and the SYBR® Green PCR Master Mix. Gene  
851 expression levels were normalized with  $\beta$ -actin as housekeeping genes. Primers used  
852 are listed in Supplementary table 1.

853 ***Protein isolation and western blot***

854 Membrane proteins from cell cultures or tissues were extracted with Lysis buffer (25  
855 mM Hepes, 4 mM EDTA, 250 mM Sucrose) containing protease inhibitor (1:000;  
856 Protease Inhibitor Cocktail Set III, EDTA-Free, Calbiochem). Briefly, tissues were  
857 lysed using the Tissue Lyser (Mini-beadbeater-16, Biospecproducts) and further  
858 centrifuged at 10000 g for 10 minutes at 4°C. After centrifuging, the supernatant was  
859 centrifuged again on an ultracentrifuge at 55000 rpm for 1 hour at 4°C. Finally, protein  
860 concentration was determined using Pierce BCA Protein Assay Kit (ThermoFisher  
861 Scientific). Membrane proteins were resolved in 10% acrylamide gels for SDS-PAGE  
862 and transferred to Immobilon membranes (Millipore). The following antibodies were  
863 used: polyclonal rabbit anti- $\gamma$ LAT1 was used at 1:750 dilution with 5% non-fat dried  
864 milk in PBS Tween-20 (0.1%) (Bodoy et al., 2019); rabbit anti-FPN1 was used at 1:250  
865 dilution with 5% non-fat dried milk in TBS Tween-20 (0.1%) (Nairz et al., 2013).  
866 Antibody binding was then detected using appropriate horseradish peroxidase (HRP)-

867 conjugated secondary antibodies (1:1000 dilution). Proteins were detected by the  
868 enhanced chemiluminescence method (GE Healthcare Life Sciences) and quantified  
869 by scanning densitometry.

870 ***Primary bone marrow macrophages (BMDMs) cell culture***

871 BM cells from 12-week-old mice (either female or male) were flushed from mice femurs  
872 and tibias. The cell suspension was lysed for 5 min in ACK lysis buffer at RT and then  
873 washed, resuspended, and cultured for 7 days in Dulbecco's Modified Eagle Medium  
874 (DMEM) supplemented with 10% heat-inactivated fetal bovine serum (FBS), 50 U/mL  
875 penicillin, 50 µg/mL streptomycin and 50 ng/mL of recombinant M-CSF (Peprotech) or  
876 30% of L-Cell (L929 supernatant (SN)) media. Six days after the seeding, cells were  
877 harvested and re-seeded with the specific conditioned media for 24 hours. To deplete  
878 arginine, arginine-free media was used (DMEM for SILAC, ThermoFisher).

879 **QUANTIFICATION AND STATISTICAL ANALYSIS**

880 Data were analyzed using GraphPad Prism Version 8 software. Statistical analysis  
881 was performed using the Student's *t* test and one- and two-way ANOVA as specified  
882 in each figure legend.

883

884 **References**

885 A-Gonzalez N, Quintana JA, García-Silva S, Mazariegos M, de la Aleja AG, Nicolás-ávila JA,  
886 Walter W, Adrover JM, Crainiciuc G, Kuchroo VK, Rothlin C V., Peinado H, Castrillo A,  
887 Ricote M, Hidalgo A. 2017. Phagocytosis imprints heterogeneity in tissue-resident  
888 macrophages. *J Exp Med* **214**:1281–1296. doi:10.1084/jem.20161375  
889 Al-Qattan S, Malcolmson C, Mercimek-Andrews S. 2021. Lysinuric protein intolerance  
890 mimicking N-acetylglutamate synthase deficiency in a nine-year-old boy. *Mol Genet*  
891 *Metab Reports* **27**:100741. doi:10.1016/j.ymgmr.2021.100741  
892 Alqarajeh F, Omorodion J, Bosfield K, Shur N, Ferreira CR. 2020. Lysinuric protein  
893 intolerance: Pearls to detect this otherwise easily missed diagnosis. *Transl Sci Rare Dis*  
894 **5**:81–86. doi:10.3233/TRD-190035  
895 Andriopoulos B, Corradini E, Xia Y, Faasse SA, Chen S, Grgurevic L, Knutson MD,  
896 Pietrangelo A, Vukicevic S, Lin HY, Babitt JL. 2009. BMP6 is a key endogenous  
897 regulator of hepcidin expression and iron metabolism. *Nat Genet* **41**:482–487.  
898 doi:10.1038/ng.335

899 Barilli A, Rotoli BM, Visigalli R, Bussolati O, Gazzola GC, Gatti R, Dionisi-Vici C, Martinelli D,  
900 Goffredo BM, Font-Llitjós M, Mariani F, Luisetti M, Dall'Asta V. 2012. Impaired  
901 phagocytosis in macrophages from patients affected by lysinuric protein intolerance.  
902 *Mol Genet Metab* **105**:585–589. doi:10.1016/j.ymgme.2012.01.008

903 Beaumont C, Delaby C. 2009. Recycling Iron in Normal and Pathological States. *Semin  
904 Hematol* **46**:328–338. doi:10.1053/j.seminhematol.2009.06.004

905 Beguin Y. 1998. Prediction of response to optimize outcome of treatment with erythropoietin.  
906 *Semin Oncol* **25**:27–34.

907 Benjamini Y, Hochberg Y. 1995. Controlling the False Discovery Rate: A Practical and  
908 Powerful Approach to Multiple Testing. *J R Stat Soc Ser B* **57**:289–300.  
909 doi:10.1111/j.2517-6161.1995.tb02031.x

910 Bennett LF, Liao C, Paulson RF. 2018. Stress erythropoiesis model systemsMethods in  
911 Molecular Biology. Humana Press Inc. pp. 91–102. doi:10.1007/978-1-4939-7428-3\_5

912 Bodoy, Sotillo, Espino-Guarch, Sperandeo, Ormazabal, Zorzano, Sebastio, Artuch, Palacín,  
913 Bodoy S, Sotillo F, Espino-Guarch M, Sperandeo MP, Ormazabal A, Zorzano A,  
914 Sebastio G, Artuch R, Palacín M. 2019. Inducible Slc7a7 Knockout Mouse Model  
915 Recapitulates Lysinuric Protein Intolerance Disease. *Int J Mol Sci* **20**:5294.  
916 doi:10.3390/ijms20215294

917 Bolstad B, Collin F, Brettschneider J, Simpson K, Cope L, Irizarry R, Speed T. 2005. Quality  
918 Assessment of Affymetrix GeneChip Data In: Gentleman R, Carey V, Huber W, Irizarry  
919 R, Dudoit S, editors. Bioinformatics and Computational Biology Solutions Using R and  
920 Bioconductor. New York, NY: Springer-Verlag. pp. 33–47. doi:10.1007/0-387-29362-  
921 0\_3

922 Bronte V, Zanovello P. 2005. Regulation of immune responses by L-arginine metabolism.  
923 *Nat Rev Immunol*. doi:10.1038/nri1668

924 Chen K, Liu J, Heck S, Chasis JA, An X, Mohandas N. 2009. Resolving the distinct stages in  
925 erythroid differentiation based on dynamic changes in membrane protein expression  
926 during erythropoiesis. *Proc Natl Acad Sci* **106**:17413–17418.  
927 doi:10.1073/pnas.0909296106

928 Chow A, Huggins M, Ahmed J, Hashimoto D, Lucas D, Kunisaki Y, Pinho S, Leboeuf M,  
929 Noizat C, Van Rooijen N, Tanaka M, Zhao ZJ, Bergman A, Merad M, Frenette PS.  
930 2013. CD169 + macrophages provide a niche promoting erythropoiesis under  
931 homeostasis and stress. *Nat Med* **19**:429–436. doi:10.1038/nm.3057

932 Cobbold SA, Llinás M, Kirk K. 2016. Sequestration and metabolism of host cell arginine by  
933 the intraerythrocytic malaria parasite *Plasmodium falciparum*. *Cell Microbiol* **18**:820–  
934 830. doi:10.1111/cmi.12552

935 Cohen LA, Gutierrez L, Weiss A, Leichtmann-Bardoogo Y, Zhang DL, Crooks DR, Sougrat  
936 R, Morgenstern A, Galy B, Hentze MW, Lazaro FJ, Rouault TA, Meyron-Holtz EG.  
937 2010. Serum ferritin is derived primarily from macrophages through a nonclassical  
938 secretory pathway. *Blood* **116**:1574–1584. doi:10.1182/blood-2009-11-253815

939 Core AB, Canali S, Babitt JL. 2014. Hemojuvelin and bone morphogenetic protein (BMP)  
940 signaling in iron homeostasis. *Front Pharmacol*. doi:10.3389/fphar.2014.00104

941 de Back DZ, Kostova EB, van Kraaij M, van den Berg TK, van Bruggen R. 2014. Of  
942 macrophages and red blood cells: a complex love story. *Front Physiol* **5**.  
943 doi:10.3389/fphys.2014.00009

944 Dhanakoti SN, Brosnan JT, Herzberg GR, Brosnan ME. 1990. Renal arginine synthesis:  
945 Studies in vitro and in vivo. *Am J Physiol - Endocrinol Metab* **259**.  
946 doi:10.1152/ajpendo.1990.259.3.e437

947 Dichtl S, Haschka D, Nairz M, Seifert M, Volani C, Lutz O, Weiss G. 2018. Dopamine  
948 promotes cellular iron accumulation and oxidative stress responses in macrophages.  
949 *Biochem Pharmacol* **148**:193–201. doi:10.1016/j.bcp.2017.12.001

950 Drakesmith H, Nemeth E, Ganz T. 2015. Ironing out Ferroportin. *Cell Metab* **22**:777–787.  
951 doi:10.1016/j.cmet.2015.09.006

952 Durinck S, Spellman PT, Birney E, Huber W. 2009. Mapping identifiers for the integration of  
953 genomic datasets with the R/ Bioconductor package biomaRt. *Nat Protoc* **4**:1184–1191.

954 doi:10.1038/nprot.2009.97

955 Efron B, Tibshirani R. 2007. On testing the significance of sets of genes. *Ann Appl Stat*  
956 1:107–129. doi:10.1214/07-AOAS101

957 Ganz T. 2012. Macrophages and Systemic Iron Homeostasis. *J Innate Immun* 4:446–453.  
958 doi:10.1159/000336423

959 Gautier L, Cope L, Bolstad BM, Irizarry RA. 2004. Affy - Analysis of Affymetrix GeneChip  
960 data at the probe level. *Bioinformatics* 20:307–315. doi:10.1093/bioinformatics/btg405

961 Gentleman RC, Carey VJ, Bates DM, Bolstad B, Dettling M, Dudoit S, Ellis B, Gautier L, Ge  
962 Y, Gentry J, Hornik K, Hothorn T, Huber W, Iacus S, Irizarry R, Leisch F, Li C, Maechler  
963 M, Rossini AJ, Sawitzki G, Smith C, Smyth G, Tierney L, Yang JYH, Zhang J. 2004.  
964 Bioconductor: open software development for computational biology and bioinformatics.  
965 *Genome Biol* 5:R80. doi:10.1186/gb-2004-5-10-r80

966 Goeman JJ, Bühlmann P. 2007. Analyzing gene expression data in terms of gene sets:  
967 Methodological issues. *Bioinformatics* 23:980–987. doi:10.1093/bioinformatics/btm051

968 Goldfarb AN, Freeman KC, Sahu RK, Elagib KE, Holy M, Arneja A, Polanowska-Grabowska  
969 R, Gru AA, White Z, Khalil S, Kerins MJ, Ooi A, Leitinger N, Luckey CJ, Delehanty LL.  
970 2021. Iron control of erythroid microtubule cytoskeleton as a potential target in  
971 treatment of iron-restricted anemia. *Nat Commun* 12. doi:10.1038/s41467-021-21938-2

972 Gonzalez-Roca E, Garcia-Albéniz X, Rodriguez-Mulero S, Gomis RR, Kornacker K, Auer H.  
973 2010. Accurate Expression Profiling of Very Small Cell Populations. *PLoS One*  
974 5:e14418. doi:10.1371/journal.pone.0014418

975 Guo M, Härtlova A, Gierliński M, Prescott A, Castellvi J, Losa JH, Petersen SK, Wenzel UA,  
976 Dill BD, Emmerich CH, Ramon Y Cajal S, Russell DG, Trost M. 2019. Triggering MSR1  
977 promotes JNK-mediated inflammation in IL-4-activated macrophages. *EMBO J* 38:1–  
978 15. doi:10.15252/embj.2018100299

979 Haldar M, Kohyama M, So AY-L, KC W, Wu X, Briseño CG, Satpathy AT, Kretzer NM, Arase  
980 H, Rajasekaran NS, Wang L, Egawa T, Igarashi K, Baltimore D, Murphy TL, Murphy  
981 KM. 2014. Heme-Mediated SPI-C Induction Promotes Monocyte Differentiation into  
982 Iron-Recycling Macrophages. *Cell* 156:1223–1234. doi:10.1016/j.cell.2014.01.069

983 Hattangadi SM, Wong P, Zhang L, Flygare J, Lodish HF. 2011. From stem cell to red cell:  
984 regulation of erythropoiesis at multiple levels by multiple proteins, RNAs, and chromatin  
985 modifications. *Blood* 118:6258–6268. doi:10.1182/blood-2011-07-356006

986 Hussell T, Bell TJ. 2014. Alveolar macrophages: plasticity in a tissue-specific context. *Nat  
987 Rev Immunol* 14:81–93. doi:10.1038/nri3600

988 Irizarry RA. 2003. Exploration, normalization, and summaries of high density oligonucleotide  
989 array probe level data. *Biostatistics* 4:249–264. doi:10.1093/biostatistics/4.2.249

990 Jd T, Th B. 1968. A simple technique for measuring storage iron concentrations in  
991 formalinised liver samples. *S Afr J Med Sci* 33:9–11.

992 Jelkmann W. 2011. Regulation of erythropoietin production. *J Physiol* 589:1251–1258.  
993 doi:10.1113/jphysiol.2010.195057

994 Jha AK, Huang SC-CC, Sergushichev A, Lampropoulou V, Ivanova Y, Loginicheva E,  
995 Chmielewski K, Stewart KM, Ashall J, Everts B, Pearce EJ, Driggers EM, Artyomov MN.  
996 2015. Network integration of parallel metabolic and transcriptional data reveals  
997 metabolic modules that regulate macrophage polarization. *Immunity* 42:419–430.  
998 doi:10.1016/j.jimmuni.2015.02.005

999 JL B, FW H, DM W, Y X, Y S, TA S, JA C, RT C, AL S, CJ W, NC A, HY L. 2006. Bone  
1000 morphogenetic protein signaling by hemojuvelin regulates hepcidin expression. *Nat  
1001 Genet* 38:531–539. doi:10.1038/NG1777

1002 Kawasumi H, Gono T, Kawaguchi Y, Kaneko H, Katsumata Y, Hanaoka M, Kataoka S,  
1003 Yamanaka H. 2014. IL-6, IL-8, and IL-10 are associated with hyperferritinemia in rapidly  
1004 progressive interstitial lung disease with polymyositis/dermatomyositis. *Biomed Res Int*  
1005 2014. doi:10.1155/2014/815245

1006 Klei TRL, Meinderts SM, van den Berg TK, van Bruggen R. 2017. From the Cradle to the  
1007 Grave: The Role of Macrophages in Erythropoiesis and Erythrophagocytosis. *Front  
1008 Immunol* 8:73. doi:10.3389/fimmu.2017.00073

1009 Knutson MD, Oukka M, Koss LM, Aydemir F, Wessling-Resnick M. 2005. Iron release from  
1010 macrophages after erythrophagocytosis is up-regulated by ferroportin 1 overexpression  
1011 and down-regulated by hepcidin. *Proc Natl Acad Sci* **102**:1324–1328.  
1012 doi:10.1073/pnas.0409409102

1013 Koh TJ, DiPietro LA. 2011. Inflammation and wound healing: the role of the macrophage.  
1014 *Expert Rev Mol Med*. doi:10.1017/S1462399411001943

1015 Kohyama M, Ise W, Edelson BT, Wilker PR, Hildner K, Mejia C, Frazier WA, Murphy TL,  
1016 Murphy KM. 2009. Role for Spi-C in the development of red pulp macrophages and  
1017 splenic iron homeostasis. *Nature* **457**:318–321. doi:10.1038/nature07472

1018 Kuhn V, Diederich L, Keller TCS, Kramer CM, Lückstädt W, Panknin C, Suvorava T, Isakson  
1019 BE, Kelm M, Cortese-Krott MM. 2017. Red Blood Cell Function and Dysfunction: Redox  
1020 Regulation, Nitric Oxide Metabolism, Anemia. *Antioxid Redox Signal* **26**:718–742.  
1021 doi:10.1089/ars.2016.6954

1022 Lee JCM, Gimm JA, Lo AJ, Koury MJ, Krauss SW, Mohandas N, Chasis JA. 2004.  
1023 Mechanism of protein sorting during erythroblast enucleation: Role of cytoskeletal  
1024 connectivity. *Blood* **103**:1912–1919. doi:10.1182/blood-2003-03-0928

1025 Liberzon A, Birger C, Thorvaldsdóttir H, Ghandi M, Mesirov JP, Tamayo P. 2015. The  
1026 Molecular Signatures Database Hallmark Gene Set Collection. *Cell Syst* **1**:417–425.  
1027 doi:10.1016/j.cels.2015.12.004

1028 Liu S, McConnell SC, Ryan TM. 2013. Erythropoiesis in the Absence of Adult Hemoglobin.  
1029 *Mol Cell Biol* **33**:2241–2251. doi:10.1128/mcb.01734-12

1030 Lukkarinen M, Näntö-Salonen K, Pulkki K, Aalto M, Simell O. 2003. Oral supplementation  
1031 corrects plasma lysine concentrations in lysinuric protein intolerance. *Metabolism*  
1032 **52**:935–938. doi:10.1016/S0026-0495(03)00089-1

1033 Luo B, Gan W, Liu Z, Shen Z, Wang J, Shi R, Liu Yuqi, Liu Yu, Jiang M, Zhang Z, Wu Y.  
1034 2016. Erythropoietin Signaling in Macrophages Promotes Dying Cell Clearance and  
1035 Immune Tolerance. *Immunity* **44**:287–302. doi:10.1016/j.immuni.2016.01.002

1036 Mauhin W, Habarou F, Gobin S, Servais A, Brassier A, Grisel C, Roda C, Pinto G, Moshous  
1037 D, Ghalim F, Krug P, Deltour N, Pontoizeau C, Dubois S, Assoun M, Galmiche L,  
1038 Bonnefont J, Ottolenghi C, de Blic J, Arnoux J, de Lonlay P. 2017. Update on Lysinuric  
1039 Protein Intolerance, a Multi-faceted Disease Retrospective cohort analysis from birth to  
1040 adulthood. *Orphanet J Rare Dis* **12**:3. doi:10.1186/s13023-016-0550-8

1041 Moestrup S, Møller H. 2004. CD163: a regulated hemoglobin scavenger receptor with a role  
1042 in the anti-inflammatory response. *Ann Med* **36**:347–354.  
1043 doi:10.1080/07853890410033171

1044 Moritz KM, Lim GB, Wintour EM. 1997. Developmental regulation of erythropoietin and  
1045 erythropoiesis. *Am J Physiol Integr Comp Physiol* **273**:R1829–R1844.  
1046 doi:10.1152/ajpregu.1997.273.6.R1829

1047 Morris SM. 2002. REGULATION OF ENZYMES OF THE UREA CYCLE AND ARGININE  
1048 METABOLISM. doi:10.1146/annurev.nutr.22.110801.140547

1049 Murray PJ, Wynn TA. 2011. Protective and pathogenic functions of macrophage subsets.  
1050 *Nat Rev Immunol* **11**:723–737. doi:10.1038/nri3073

1051 Nairz M, Schleicher U, Schroll A, Sonnweber T, Theurl I, Ludwiczek S, Talasz H,  
1052 Brandacher G, Moser PL, Muckenthaler MU, Fang FC, Bogdan C, Weiss G. 2013.  
1053 Nitric oxide–mediated regulation of ferroportin-1 controls macrophage iron homeostasis  
1054 and immune function in *Salmonella* infection. *J Exp Med* **210**:855–873.  
1055 doi:10.1084/jem.20121946

1056 Nemeth E, Ganz T. 2009. The Role of Hepcidin in Iron Metabolism. *Acta Haematol* **122**:78–  
1057 86. doi:10.1159/000243791

1058 Nemeth E, Tuttle MS, Powelson J, Vaughn MB, Donovan A, Ward DM, Ganz T, Kaplan J.  
1059 2004. Hepcidin regulates cellular iron efflux by binding to ferroportin and inducing its  
1060 internalization. *Science* **306**:2090–3. doi:10.1126/science.1104742

1061 Oexle H, Kaser A, Möst J, Bellmann-Weiler R, Werner ER, Werner-Felmayer G, Weiss G.  
1062 2003. Pathways for the regulation of interferon- $\gamma$ -inducible genes by iron in human  
1063 monocytic cells. *J Leukoc Biol* **74**:287–294. doi:10.1189/jlb.0802420

1064 Ogier de Baulny H, Schiff M, Dionisi-Vici C. 2012. Lysinuric protein intolerance (LPI): a multi  
1065 organ disease by far more complex than a classic urea cycle disorder. *Mol Genet  
1066 Metab* **106**:12–7. doi:10.1016/j.ymgme.2012.02.010

1067 Oldenborg P-A. 2000. Role of CD47 as a Marker of Self on Red Blood Cells. *Science (80- )*  
1068 **288**:2051–2054. doi:10.1126/science.288.5473.2051

1069 Palacín M, Borsani G, Sebastio G. 2001. The molecular bases of cystinuria and lysinuric  
1070 protein intolerance. *Curr Opin Genet Dev* **11**:328–335. doi:10.1016/S0959-  
1071 437X(00)00198-2

1072 Palacín M, Nunes V, Font-Llitjós M, Jiménez-Vidal M, Fort J, Gasol E, Pineda M,  
1073 Feliubadaló L, Chillarón J, Zorzano A. 2005. The Genetics of Heteromeric Amino Acid  
1074 Transporters. *Physiology* **20**:112–124. doi:10.1152/physiol.00051.2004

1075 Park SY, Kim IS. 2017. Engulfment signals and the phagocytic machinery for apoptotic cell  
1076 clearance. *Exp Mol Med*. doi:10.1038/emm.2017.52

1077 Parto K, Maki J, Pelliniemi LJ, Simell O. 1994. Abnormal pulmonary macrophages in  
1078 lysinuric protein intolerance: Ultrastructural, morphometric, and x-ray microanalytic  
1079 study. *Arch Pathol Lab Med* **118**:536–541.

1080 Patel BN, Dunn RJ, Jeong SY, Zhu Q, Julien JP, David S. 2002. Ceruloplasmin regulates  
1081 iron levels in the CNS and prevents free radical injury. *J Neurosci* **22**:6578–6586.  
1082 doi:10.1523/jneurosci.22-15-06578.2002

1083 Perkins CP, Mar V, Shutter JR, Castillo J Del, Danilenko DM, Medlock ES, Ponting IL,  
1084 Graham M, Stark KL, Zuo Y, Cunningham JM, Bosselman RA. 1997. Anemia and  
1085 perinatal death result from loss of the murine ecotropic retrovirus receptor mCAT-1.  
1086 *Genes Dev* **11**:914–925. doi:10.1101/gad.11.7.914

1087 Pollard JW. 2009. Trophic macrophages in development and disease. *Nat Rev Immunol*  
1088 **9**:259–270. doi:10.1038/nri2528

1089 Popova EY, Krauss SW, Short SA, Lee G, Villalobos J, Etzell J, Koury MJ, Ney PA, Chasis  
1090 JA, Grigoryev SA. 2009. Chromatin condensation in terminally differentiating mouse  
1091 erythroblasts does not involve special architectural proteins but depends on histone  
1092 deacetylation. *Chromosom Res* **17**:47–64. doi:10.1007/s10577-008-9005-y

1093 Posey JE, Burrage LC, Miller MJ, Liu P, Hardison MT, Elsea SH, Sun Q, Yang Y, Willis AS,  
1094 Schlesinger AE, Bacino CA, Lee BH. 2014. Lysinuric protein intolerance presenting with  
1095 multiple fractures. *Mol Genet Metab Reports* **1**:176–183.  
1096 doi:10.1016/j.ymgmr.2014.03.004

1097 R Core T. 2019. R: A language and environment for statistical computing. R Foundation for  
1098 Statistical Computing. Vienna, Austria. <https://www.r-project.org/>.

1099 Rajantie J, Simell O, Rapola J, Perheentupa J. 1980. Lysinuric protein intolerance: A two-  
1100 year trial of dietary supplementation therapy with citrulline and lysine. *J Pediatr* **97**:927–  
1101 932. doi:10.1016/S0022-3476(80)80422-7

1102 Recalcati S, Locati M, Gammella E, Invernizzi P, Cairo G. 2012. Iron levels in polarized  
1103 macrophages: Regulation of immunity and autoimmunity. *Autoimmun Rev*.  
1104 doi:10.1016/j.autrev.2012.03.003

1105 Ritchie ME, Phipson B, Wu D, Hu Y, Law CW, Shi W, Smyth GK. 2015. Limma powers  
1106 differential expression analyses for RNA-sequencing and microarray studies. *Nucleic  
1107 Acids Res* **43**:e47. doi:10.1093/nar/gkv007

1108 Rosário C, Zandman-Goddard G, Meyron-Holtz EG, D'Cruz DP, Shoenfeld Y. 2013. The  
1109 Hyperferritinemic Syndrome: macrophage activation syndrome, Still's disease, septic  
1110 shock and catastrophic antiphospholipid syndrome. *BMC Med* **11**:185.  
1111 doi:10.1186/1741-7015-11-185

1112 Rotoli BM, Barilli A, Visigalli R, Ferrari F, Dall'Asta V. 2020. y+LAT1 and y+LAT2 contribution  
1113 to arginine uptake in different human cell models: Implications in the pathophysiology of  
1114 Lysinuric Protein Intolerance. *J Cell Mol Med* **24**:921–929. doi:10.1111/jcmm.14801

1115 Sebastiani G, Wilkinson N, Pantopoulos K. 2016. Pharmacological targeting of the  
1116 hepcidin/ferroportin axis. *Front Pharmacol* **7**:1–11. doi:10.3389/fphar.2016.00160

1117 Shima Y, Maeda T, Aizawa S, Tsuboi I, Kobayashi D, Kato R, Tamai I. 2006.  
1118 HEMATOPOIESIS L -arginine import via cationic amino acid transporter CAT1 is

1119 essential for both differentiation and proliferation of erythrocytes. *Blood* **107**:1352–1356.  
1120 doi:10.1182/blood-2005-08-3166.Reprints

1121 Smyth GK. 2004. Linear models and empirical bayes methods for assessing differential  
1122 expression in microarray experiments. *Stat Appl Genet Mol Biol* **3**. doi:10.2202/1544-  
1123 6115.1027

1124 Soares MP, Hamza I. 2016. Macrophages and Iron Metabolism. *Immunity*.  
1125 doi:10.1016/j.jimmuni.2016.02.016

1126 Stienstra R, Netea-Maier RT, Riksen NP, Joosten LAB, Netea MG. 2017. Specific and  
1127 Complex Reprogramming of Cellular Metabolism in Myeloid Cells during Innate  
1128 Immune Responses. *Cell Metab*. doi:10.1016/j.cmet.2017.06.001

1129 Swartz KL, Wood SN, Murthy T, Ramirez O, Qin G, Pillai MM, Rao S, Minella AC. 2017.  
1130 E2F-2 Promotes Nuclear Condensation and Enucleation of Terminally Differentiated  
1131 Erythroblasts. *Mol Cell Biol* **37**. doi:10.1128/mcb.00274-16

1132 Theurl I, Hilgendorf I, Nairz M, Tymoszuk P, Haschka D, Asshoff M, He S, Gerhardt LMS,  
1133 Holderried TAW, Seifert M, Sopper S, Fenn AM, Anzai A, Rattik S, McAlpine C, Theurl  
1134 M, Wieghofer P, Iwamoto Y, Weber GF, Harder NK, Chousterman BG, Arvedson TL,  
1135 McKee M, Wang F, Lutz OMD, Rezoagli E, Babitt JL, Berra L, Prinz M, Nahrendorf M,  
1136 Weiss G, Weissleder R, Lin HY, Swirski FK. 2016. On-demand erythrocyte disposal  
1137 and iron recycling requires transient macrophages in the liver. *Nat Med* **22**:945–951.  
1138 doi:10.1038/nm.4146

1139 Torrents D, Mykkänen J, Pineda M, Feliubadaló L, Estévez R, de Cid R, Sanjurjo P, Zorzano  
1140 A, Nunes V, Huoponen K, Reinikainen A, Simell O, Savontaus M-LL, Aula P, Palacín  
1141 M, Cid Rafael de, Sanjurjo P, Zorzano A, Nunes V, Huoponen K, Reinikainen A, Simell  
1142 O, Savontaus M-LL, Aula P, Palacín M, de Cid R, Sanjurjo P, Zorzano A, Nunes V,  
1143 Huoponen K, Reinikainen A, Simell O, Savontaus M-LL, Aula P, Palacín M. 1999.  
1144 Identification of SLC7A7, encoding y<sup>+</sup>LAT-1, as the lysinuric protein intolerance gene.  
1145 *Nat Genet* **21**:293–296. doi:10.1038/6809

1146 Weiss G, Schaible UE. 2015. Macrophage defense mechanisms against intracellular  
1147 bacteria. *Immunol Rev* **264**:182–203. doi:10.1111/imr.12266

1148 Wu D, Lim E, Vaillant F, Asselin-Labat ML, Visvader JE, Smyth GK. 2010. ROAST: Rotation  
1149 gene set tests for complex microarray experiments. *Bioinformatics* **26**:2176–2182.  
1150 doi:10.1093/bioinformatics/btq401

1151